Manufacturing of High-Efficiency Bi-Facial Tandem Concentrator Solar Cells

February 20, 2009 — August 20, 2010

Steven Wojtczuk
Spire Semiconductor Corporation, LLC
Hudson, New Hampshire

NREL is a national laboratory of the U.S. Department of Energy, Office of Energy Efficiency & Renewable Energy, operated by the Alliance for Sustainable Energy, LLC.

Subcontract Report
NREL/SR-5200-51767
June 2011

Contract No. DE-AC36-08GO28308

NATIONAL RENEWABLE ENERGY LABORATORY

Manufacturing of High-Efficiency Bi-Facial Tandem Concentrator Solar Cells

February 20, 2009 — August 20, 2010

Steven Wojtczuk

Spire Semiconductor Corporation, LLC
Hudson, New Hampshire

NREL Technical Monitor: Harin S. Ullal

Prepared under Subcontract No. NAT-9-88012-04

National Renewable Energy Laboratory
1617 Cole Boulevard
Golden, Colorado 80401
303-275-3000 • www.nrel.gov

Subcontract Report
NREL/SR-5200-51767
June 2011

Contract No. DE-AC36-08GO28308

Available electronically at http://www.osti.gov/bridge

Available for a processing fee to U.S. Department of Energy
and its contractors, in paper, from:

U.S. Department of Energy
Office of Scientific and Technical Information

P.O. Box 62
Oak Ridge, TN 37831-0062
phone: 865.576.8401
fax: 865.576.5728
email: mailto:reports@adonis.osti.gov

Available for sale to the public, in paper, from:

U.S. Department of Commerce
National Technical Information Service
5285 Port Royal Road
Springfield, VA 22161
phone: 800.553.6847
fax: 703.605.6900
email: orders@ntis.fedworld.gov
online ordering: http://www.ntis.gov/help/ordermethods.aspx

Cover Photos: (left to right) PIX 16416, PIX 17423, PIX 16560, PIX 17613, PIX 17436, PIX 17721

Printed on paper containing at least 50% wastepaper, including 10% post consumer waste.

Table of Contents

1 Executive Summary

Spire Semiconductor made concentrator photovoltaic (CPV) cells using a new bi-facial growth process and met both main program goals:

a) 42.5% efficiency 500X (AM1.5D, 25C, 100mW/cm^2)
b) Ready to supply at least 3MW/year of such cells at end of program.

We explored a unique simple fabrication process to make a N/P 3-junction InGaP/GaAs/InGaAs tandem cells[1]. First, the InGaAs bottom cell is grown on the back of a GaAs wafer. The wafers are then loaded into a cassette, spin-rinsed to remove particles, dipped in dilute NH4OH and spin-dried. The wafers are then removed from the cassette loaded the reactor for GaAs middle and InGaP top cell growth on the opposite wafer face (bi-facial growth). By making the epitaxial growth process a bit more complex, we are able to avoid more complex processing (such as large area wafer bonding or epitaxial liftoff) used in the inverted metamorphic (IMM) approach to make similar tandem stacks. We believe the yield is improved compared to an IMM process. After bi-facial epigrowth, standard III-V cell steps (back metal, photolithography for front grid, cap etch, AR coat, dice) are used in the remainder of the process.

1.1 Final Cell Performance

NREL measurement of a large (~1cm^2) bi-facial growth cell was 42.2% at 500X (Figure 1) with a measurement error such that it is arguable that the 42.5% program goal was met. This cell has the highest efficiency ever reported by NREL (42.3% at 505 suns, AM1.5D, 25C).

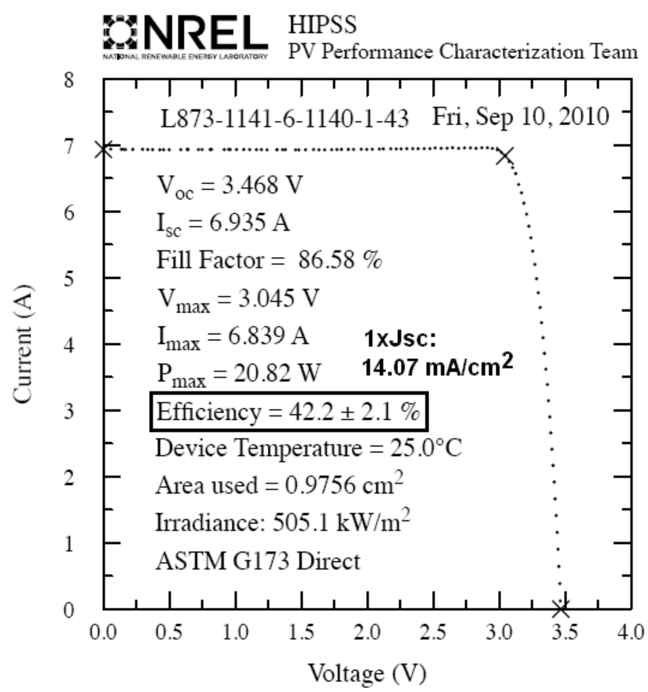

Figure 1. NREL-measured illuminated IV of record-efficiency Spire Semiconductor cell.

1.2 6MW/Year Capability

An estimate of the cell throughput (>6MW/year) with present equipment and facilities follows:

- Each 0.97cm^2 photoarea cell outputs 500X x 0.1W/cm^2 x 42.5% or 20.6W.
- There are 52 0.97cm^2 cells on a 4in wafer, so up to 1070W is available per wafer.
- The Veeco (Emcore) E450 program epigrowth reactor grows 13 4in wafers per run.
- Two complete bi-facial growths can be done in two shifts (26 wafers or ~27.8kW/16 hrs).
- 3000kW/27.8kW/(2-shift day) or 135 days (if 80% yield) are needed to grow cells.
- A resource efficient batch size in our present non-optimized wafer fab is 13 wafers.
- We could finish 2 wafer batches/day for 135 days to make 3MW of cells (>6MW/year).

2 Background

2.1 Overview of Competing Technologies

High efficiency III-V concentrator photovoltaic (CPV) cells are generally based on the two junction $In_{0.49}Ga_{0.51}P$/GaAs cell pioneered by NREL's Jerry Olson, Sarah Kurtz, et al.[2]. This cell was commercially adapted for use as one sun space solar cells by Spectrolab and Emcore (which acquired ASEC/Tecstar). A third junction was added in the Ge wafer used for III-V space cells for mechanical robustness. These companies have adapted this triple-junction InGaP/GaAs/Ge cell for CPV use, producing fine concentrator cells with the best cells having a record efficiency of 41.6% at 364X, 25C[3]. However, the Ge has too low a bandgap for optimal use in lattice-matched InGaP/GaAs tandems. The Ge's high Jsc (~20mA/cm^2 AM1.5D, 100mW/cm^2) is current mismatched to the InGaP and GaAs subcells (~15mA/cm^2) while the low Ge bandgap also gives less Voc and a lower FF than a higher, more optimal bandgap bottom subcell. One should be able to do better with a different scheme.

One approach to improve the InGaP/GaAs/Ge three junction tandem is to adjust the material compositions and therefore bandgaps of the upper and middle cell for better current matching, trading off the improvement in overall Jsc with some efficiency decrease due to the minority-carrier lifetime-lowering dislocation defects from the lattice mismatch to the Ge in the upper and middle cells (Figure 2). With this approach, $In_{0.65}Ga_{0.35}P/In_{0.17}Ga_{0.83}As$/Ge metamorphic cells with 1.1% mismatch were made with efficiency up to 41.1% at 454X by Fraunhofer[4].

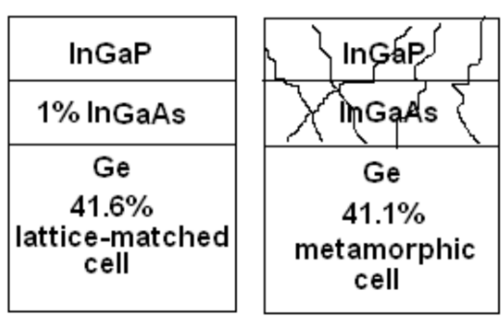

Figure 2. Left: lattice-matched InGaP/GaAs/Ge cell. Right: metamorphic cell with better Jsc but lower Voc. Dislocations indicated by squiggly lines.

Another approach to achieve higher efficiency is to substitute lattice-mismatched InGaAs for the Ge bottom cell (a "Ge-free" approach). The inverted metamorphic (IMM) process (Figure 3) can maintain lattice match for the top and middle cell by growing an inverted cell stack with the lattice mismatched InGaAs cell last. Dislocations in the InGaAs thread upward during growth, so that the top and middle cells can remain defect-free. Geisz et al.[5] used a variation of this IMM technique with a slightly mismatched middle cell to achieve 40.8% at 326X from a 0.7% mismatch $In_{0.49}Ga_{0.51}P/In_{0.04}Ga_{0.96}As/In_{0.37}Ga_{0.63}As$ cell.

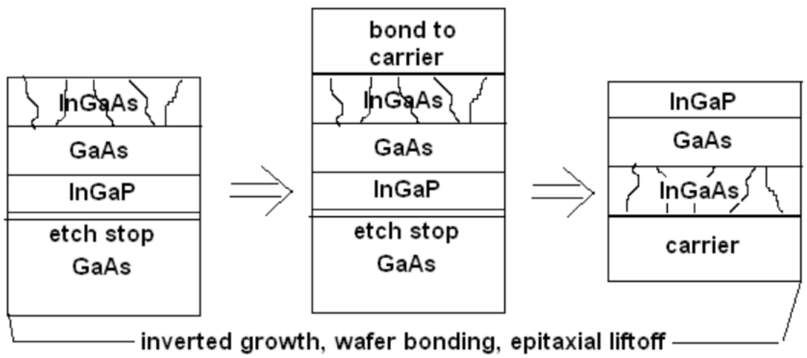

Figure 3. IMM process: Inverted growth; wafer bond to carrier; epitaxial liftoff and flip.

There are approaches (such as the VHESC program championed by Dr. Barnett) pursuing a mechanical stack multijunction approach[6], which promise efficiencies of 55%. These programs use a mechanical stack of 4 or more separate cells, or a lateral approach in which the cells are placed side-by-side and the spectrum is split and re-directed onto the proper cell. The argument for the proposed cell versus such a competitor would be we believe a reliable high yield single 42.5% cell should be more cost-effective than a 55% mechanically complex approach using multiple (4 or more) cell die.

2.2 Overview of Spire's Bi-Facial Growth Process

Spire Semiconductor's bi-facial (epitaxial) growth (BFG) process[1] (Figure 4) makes a similar InGaP/GaAs/InGaAs tandem cell without using whole-area wafer bonding and epitaxial liftoff steps which are not standard III-V cell process steps and may be low yield. The dislocations of the lattice mismatched cell are isolated from affecting the middle and top cells on the opposite wafer side by the thick GaAs wafer. Also, no carrier wafer is needed as in the IMM approach.

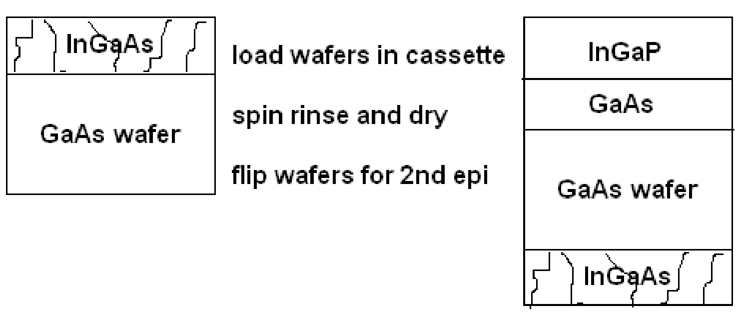

Figure 4. Bi-facial process: grow InGaAs cell on back, rinse and dry wafer to clean particles, flip wafer, and grow rest of cell. InGaAs illuminated through wafer.

A bi-facial epigrowth cell was first described by Varian[7] in 1990. They discuss an AlGaAs/GaAs/InGaAs tandem and clearly describe the idea of "farside" wafer growth, but did not actually make a bi-facial cell. In 2005, King[8] refers to the Varian work and has a cross-section of the idea of a bi-facial InGaP/GaAs/InGaAs cell, but no cell was made. Finally, Wanlass[9] has considered bi-facial cells for InGaAsP/InP wafer/InGaAs tandems.

2.3 Commercialization Issues

Commercialization of the bi-facial epigrowth of InGaP/GaAs/InGaAs tandems faces 3 hurdles.

First, the cells have to be more efficient than the "standard" InGaP/GaAs/Ge tandem technology that set a past record efficiency of 41.6% at 364X. We have exceeded this efficiency (42.3% at 406X, 42.2% at 505X, 25C, AM1.5D). Since we have been working on the basics of the bi-facial epigrowth tandem for only about 18 months and have exceeded or equaled the results of the InGaP/GaAs/Ge cell technology that has been under development for almost twenty years, we feel the approach has promise. There is still potential for efficiency improvement as the subcell dopings, thicknesses and compositions are not fully optimized.

Second, the cells have to be as reliable as the InGaP/GaAs/Ge technology. The cells have passed minimal reliability requirements of this program and more extensive reliability testing required by module manufacturers is on-going.

Third, the cells must have high yield and be cost-effective. The process is simple compared with the IMM approach (no wafer-scale epitaxial liftoff or wafer bonding or carrier substrates) and is similar to the standard lattice-matched InGaP/GaAs/Ge process. Since the yield will be similar and it comes down to arguments about the cost of GaAs vs Ge wafers and epigrowth time.

In moderate quantities, GaAs and Ge wafer costs seem similar (~$80/4in wafer in quantities >30,000/yr circa 2010). The epigrowth is longer in the bifacial process than for lattice-matched InGaP/GaAs/Ge because of time added for the InGaAs cell as opposed to the junction in Ge being formed by dopant diffusion during the growth of the III-V cells. This added growth cost must be balanced against whatever efficiency benefit is ultimately achieved. However, the growth times would be much closer if lattice-mismatched metamorphic InGaP/GaAs/Ge cells became the new production standard for Ge-based cells.

2.4 Space Applications

It is unlikely that InGaP/GaAs/InGaAs tandems made with this bi-facial growth process would be useful as ***one-sun*** space cells. Near-infrared-transparent GaAs wafers are needed so the bottom cell can receive light. A Ge wafer, preferred for space applications versus GaAs due to its mechanical strength, would absorb this 890-1300nm infrared light, so GaAs wafers must be used. Although the densities of GaAs and Ge are similar, the Ge strength allows use of thinner wafers and therefore higher W/kg numbers in one-sun systems. However, these cells could be useful in space concentrator systems where, for a given power, the required cell area is smaller by the concentration factor, and a thicker GaAs substrate on the cell may not be as significant a weight penalty versus a one-sun system.

3 First-Order Modeling: Roadmap to 42.5% Cell

Table 1 shows the final “roadmap” to the 42.5% goal which was updated throughout the program and used to indicate which subcells were on target or needed improvement. Table 1 compares model vs measured data from single junction (1J) subcells and 3J tandems. The data is normalized to 1cm^2. 1J subcells are easier to analyze. The GaAs subcell includes both tunnel junctions (TJs) and has an integrated InGaP filter of the same thickness as the top cell (to mimic TJ dopant diffusion). The InGaAs subcell is illuminated through the GaAs wafer.

Table 1. “Roadmap” for a >42% Concentrator

Subcell Perfomance Models	***Top***	***Middle***	***Bottom***	Comments
Subcell Wafer IDs	1115-2	1051-1	1140-10	
Material	InGaP	GaAs*	InGaAs	*GaAs has thin 1%InGaAs to extend cutoff
Bandgap (eV)	1.88	1.424	0.93	
λ_I cut-on (nm)	370	670	890	Cut-on and cutoff wavelengths approximate
λ_F cut-off (nm)	660	890	1330	
Upper limit Jsc: (100%) QE (λ_I to λ_F)	16.51	15.54	19.27	conditon: AM1.5D 0.1W/cm^2
Measured 1xJsc by Illuminated IV (CW)	14.22	14.20	14.32	wafer avg: CW sim adj by 3 filtered ref cells
"Boxcar" Average QE (flat from λ_I to λ_F)	0.86	0.91	0.74	(measured Jsc)/(100% QE Jsc)
Jsc Average Loss Analysis				
Grid shadow (4μ lines, 115μ gaps, wings)	0.03	0.03	0.03	SEM: liftoff Au lines 2um on top, 4um at base
Measured Avg. AR Refl. (λ_I to λ_F)	0.067	0.019	0.061	avg of Optronics QE test set refl data
20nm InAlP window loss (50% collection)	0.026			0.43mA loss calculated from InAlP n k data
20nm GaAs TJ absorption		0.028		0.44mA loss calculated from GaAs n k data
GaAs wafer absorption			0.067	1.3mA loss calculated from GaAs n k data
Collection (diffusion length) Loss	0.02	0.01	0.10	Estimate: adjusted to fit measured Jsc
Sum of Losses	0.14	0.09	0.26	sum of losses equals to 1 - Boxcar QE
Model 1xJsc (mA/cm^2)	14.2	14.2	14.3	
500xJsc (A/cm^2)		7.1		
Dark current I_O prefactor D (A/cm^2/K^3)	0.008	0.003	0.035	
I_O: DT^{3}exp(-Eg/kT) (A/cm^2)	3.6E-27	6.9E-20	1.8E-10	compare to radiative limit below
Shockley Radiative Limit - absorbing wafer	*3.1E-28*	*1.2E-20*	*9.4E-13*	q (2πkT/h^{2}c^3) (nr^2+1) Eg^2 exp(-Eg/kT) (A/cm^2)
Model 1xVoc (V) at 25C	1.455	1.025	0.468	nr is refractive index in above equation
Model 500xVoc (V) at 25C	1.615	1.184	0.627	D adjusted to fit to measured 500xVoc
Data from:		**NREL**	**NREL**	
Process Lot ID:		**L810**	**L873**	
InGaP/GaAs epirun ID:		**0952-3**	**1141-6**	
InGaAs epirun ID:		**0951-3**	**1140-1**	
Cell ID on Wafer:		**15**	**43**	
Model vs Best Cell Data				
Tandems	model	**Dlvy D09**	**Dlvy D11**	
1xJsc (mA/cm^2)	14.2	**13.63**	**14.07**	target (model) average vs "best cell" data
500xJsc (A/cm^2)	7.1	**6.8**	**7.0**	
1xVoc (V)	2.948			
500xVoc (V)	3.427	**3.495**	**3.468**	
Rs and FF Analysis				
Calc. Emitter R (Ω-cm^2)	0.006			Measured 500 Ω/sq emitter Rsh
Calc. Grid R (Ω-cm^2)	0.008			Calculated 0.005 Ω/sq Au grid metal Rsh
Est. 2 TJs (Ω-cm^2)	0.003			2.5mΩ for 20nm upper +0.5mΩ for 30nm lower TJ
Sum of series Rs (Ω-cm^2)	0.017			
Ideality "n" (3J)	3			assume n=1 per junction
1xFF	0.880			model: v=qVoc/(nkT); r=V/Jm; rs=Rs/r
500xFF	0.862	**0.851**	**0.866**	FF = ([v-ln(v+1)]/(1+v)) (1 - rs)
1xEff	0.368			
500xEff	0.419	**0.41**	**0.42**	

Tandem efficiency is determined by the quantum efficiency, dark currents, and series resistance of the subcells. Table 1 indicates the average QE for each subcell, obtained as the ratio of the measured 1xJsc from a simulator IV measurement and the 1xJsc that would be obtained over the response range if perfect QE using ASTM G173 data. Although using the complete spectral response is more accurate, the average QE allows for quick back-of-the envelope calculations useful during the program. The Jsc loss analysis indicates the relative importance of losses, including InAlP window, GaAs tunnel junction layer, and GaAs substrate absorption for the top, middle, and bottom cells respectively. Collection efficiency of the InGaAs bottom cell is much higher than the other subcells due to dislocations shortening the diffusion lengths.

The dark current in Table 1 is empirically adjusted to match the measured wafer Voc averages of the component subcells at 500X concentration. Subcell dark current for the top and middle cells is within 10X of the Shockley-Queisser radiative limit, as modified by Henry[10] for an absorptive substrate. This means we cannot do much better with Voc except for the InGaAs bottom cell, which is 200X higher than the limit due to the presence of dislocations.

4 Cell Discussion

4.1 Anti-Reflection (AR) Coating

In this program, we examined the following AR films (refractive indices at 632nm):

- MgF_2: n ~ 1.38 (e-beam and thermal)
- SiO_2: n ~ 1.46 (PECVD and e-beam)
- Al_2O_3: n ~ 1.6 (e-beam)
- SiN(H): n adjustable 1.8 to 2.3 (PECVD); n > 2.0 has absorption below 500nm
- Ta_2O_5: n ~ 2.0
- ZnS: n ~ 2.35 (e-beam and thermal)
- TiO_2: n ~ 2.35 (e-beam, using Ti_3O_5 source)

Originally, we planned to use a robust PECVD SiO_2/SiNH AR coating, but the non-stochiometric SiNH had substantial absorption below 500nm for higher (Si-rich) indices. We then decided to use MgF_2/ZnS for cells working into air and evaporated SiO_2/ZnS for cells under glass. The SiO_2 AR film will be part of a semi-infinite medium when used with index-matched epoxy and a thick coverglass. We experimented with Ta_2O_5 and TiO_2 to see if we could get a higher index (and broader bandwidth) coating, but although higher indices have been reported in the literature, we obtained lower indices and erratic results compared to the ZnS. We solve the issue of patterning the AR by use of an image reversal photolithography step prior to the MgF_2/ZnS coating. Figure 5 shows the final program AR coat on a three junction tandem, a two junction (diagnostic) tandem with no InGaAs bottom cell (note high reflection off metal on back of GaAs wafer in IR), and a model. The model InGaAs optical constant data file available is for an InGaAs composition of a slightly higher bandgap than the final cells so the IR cutoff is in error.

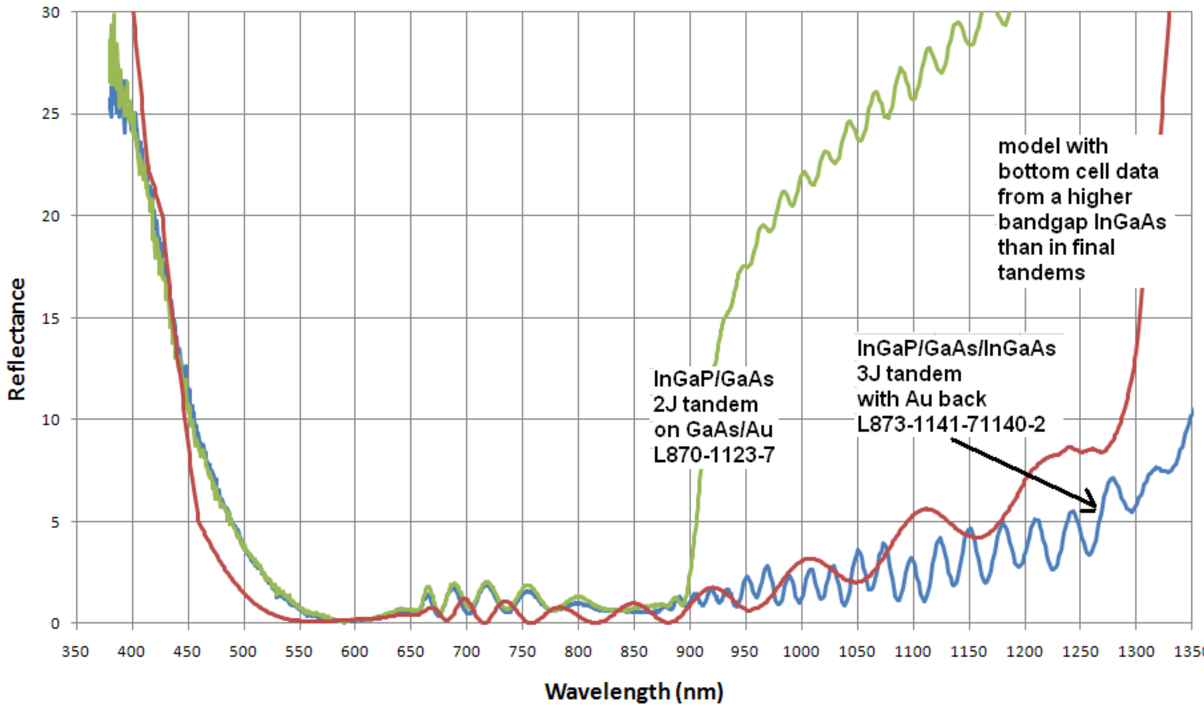

Figure 5. Measured reflectance (120nm MgF2/60nm ZnS) on 3J & 2J tandem vs model.

4.2 Top Contact Grid Design

We wanted to use Ag for the contact grid of final program cells because it is about 50% more conductive than Au and would be more economical in production. However. we were stymied by erratic Jsc data for cells with Ag gridlines. We use a self-aligned contact cap etch process in which we first create a liftoff profile (dovetail) in photoresist using an ammonia-doped image reversal process, evaporate 5µm of metal, and liftoff the excess metal in acetone. Prior to AR coating, we etch the heavily doped N GaAs contact cap layer in a selective citric acid etch that removes the GaAs everywhere but under the metal gridlines and stops on the InAlP window. We do not use the popular ammonium hydroxide/hydrogen peroxide selective etch because it badly attacks Ag. However, although this citric process works well for inert Au gridlines, more reactive Ag gridlines seem to leave varying amounts of the cap or some other residue next to the gridlines (Figure 6). For commercial reasons, we are still working on developing the Ag grid process, but the delivered program cells use tapered Au gridlines similar to Figure 7.

Figure 8 shows a top view of the final program cell. An optimum four busbar design of the type shown has appreciably less grid I^2R loss and the same grid shadow and emitter I^2R loss than a similar simpler optimum two busbar parallel line design employed on occasion earlier in the program. The grid design is optimal when the details of the grid line shape and measured metal and emitter sheet resistance are taken into account as in the in the grid loss analysis and optimization presented below (Figure 8).

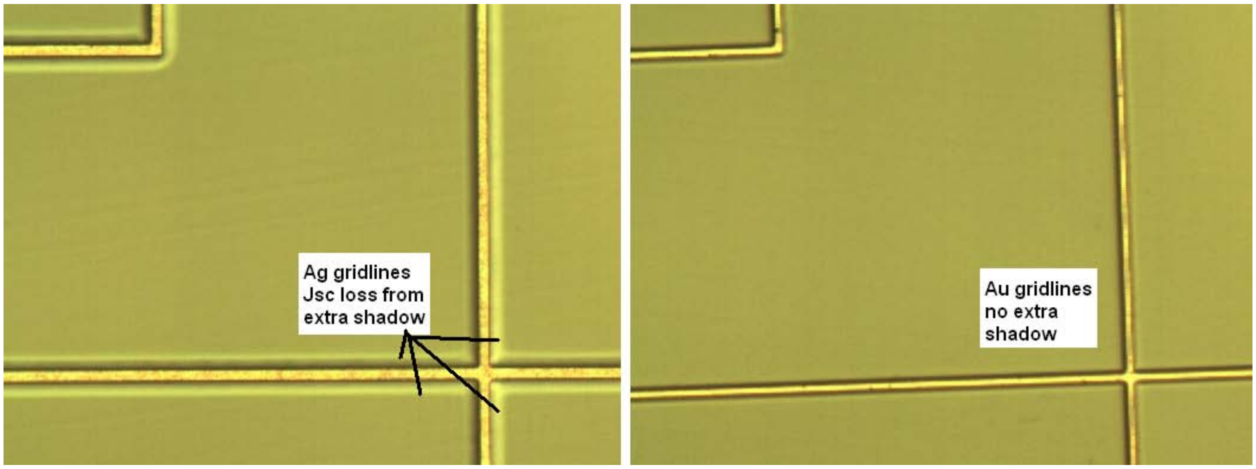

Figure 6. Comparison of 4μm wide Ag and Au gridlines after cap etch and AR coating. Note the extra "shadow" around the Ag gridlines that is absent from the Au gridlines after the same cap etch. Credit: Spire.

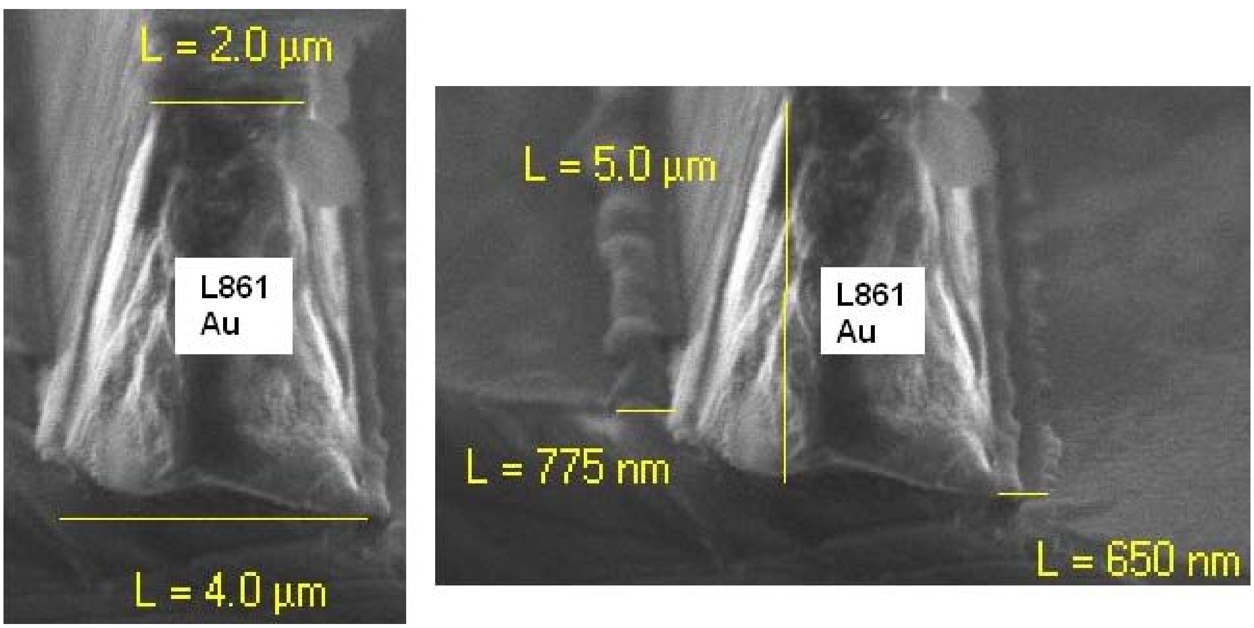

Figure 7. 5μm high Au gridline with 2μm top, 4μm base, and ~0.7μm "wings" off base. Credit: Spire.

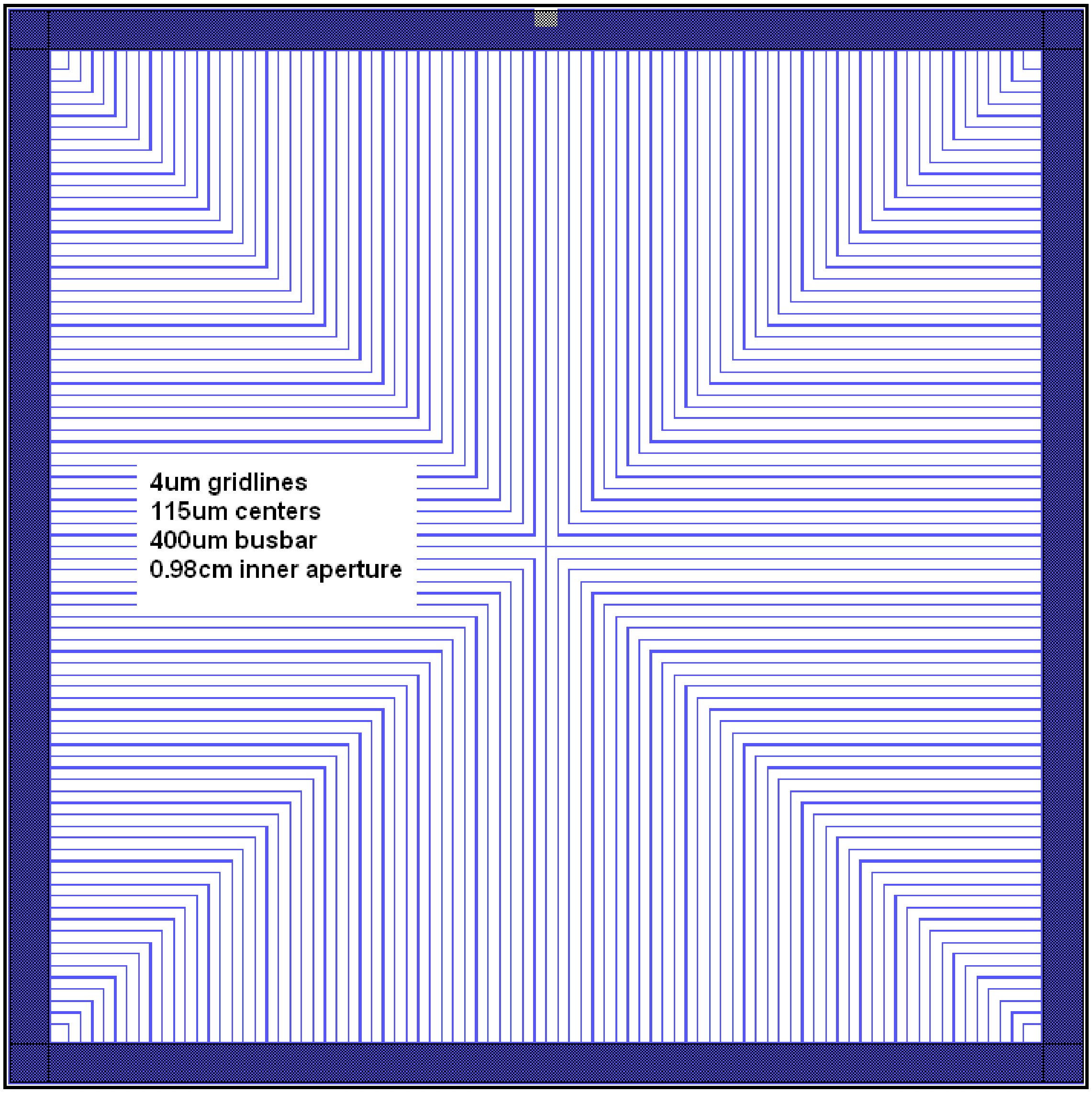

Figure 8. Top view of the four busbar program cell.

The fill factor analysis used in the roadmap is based on a standard analysis described most clearly by Green[11]. The calculation of the series resistance needed from the grid metal and emitter sheet power loss is shown in Figure 9 after the gridline spacing optimization using data for cells at the end of the program. The model for the gridline shadow is based on the SEM images taken of the program liftoff process Au gridlines, which are tapered (2μm at top and 4μm at bottom) as shown in Figure 7. Some of the benefit of these tapered lines (some light hitting tapered sidewall is reflected onto cell and not lost) is reduced by the presence of the unfortunate "wings" which are roughly 0.7μm per side residue at foot of gridline which contribute shadow but no significant current conduction capability.

Tapered grid X-section design for square cell with 4 busbars assuming uniform illumination

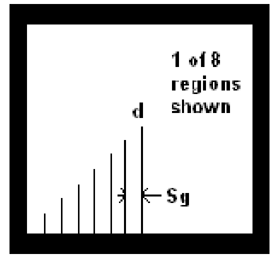

Suns	$Suns := 500$	Power density	$Pdens := 0.1 W\cdot cm^{-2}$		
Pin	$Pin := Suns\cdot Pdens = 50\cdot W\cdot cm^{-2}$	Gridline thick.	$tg := 5\cdot\mu m$		
1xJmax	$Jm1 := 13.8 mA\cdot cm^{-2}$	Gridline ρ	$\rho := 2.35\cdot 10^{-6}\cdot\Omega\cdot cm$		
Jmax	$Jm := Suns\cdot Jm1 = 6.9\cdot A\cdot cm^{-2}$		$m\Omega := 0.001\Omega$ $\quad x := 1..4$		
1xJsc	$Jsc1 := 14 mA\cdot cm^{-2}$	Top of Gridline	$d_x := x\cdot\mu m$		
Jsc	$Jsc := Suns\cdot Jsc1 = 7\cdot A\cdot cm^{-2}$	base of gridline - top	$\Delta := 2\mu m$	Cell Side	$Wc := 10mm$
Vmax	$Vm := 3\cdot V$	Base of gridline	$base_x := d_x + \Delta$	Estimated cell ideality	$n := 3.2$
Voc	$Voc := 3.5V$	Gridline wing	$dw := 0.7\mu m$	# of lines per segment	$i := 2..100$
Emitter Rsh	$Rshe := 500\Omega$	Line X-sect Area	$A_{g_x} := 0.5\cdot(d_x + base_x)\cdot tg$	Grid Spacing	$Sg_i := \frac{Wc}{2\cdot i}$

model for 8 similar triangular sectors; gridline spacing also determines line length; busbar loss is for 4 probes at center of busbars

$$Pshad_{i,x} := 8\cdot Vm\cdot Jm\cdot(d_x + 2\cdot dw)\cdot\left[\sum_{n=1}^{i}(n\cdot Sg_i) - \frac{Wc}{4}\right] \qquad Pemit_i := 8\cdot\sum_{n=1}^{i}\int_{-0.5\cdot Sg_i}^{0.5\cdot Sg_i}(Jm\cdot n\cdot Sg_i\cdot x)^2\cdot\frac{Rshe}{n\cdot Sg_i}\,dx \qquad \%Sh_{i,x} := \frac{100\cdot Pshad_{i,x}}{Pin\cdot Wc^2}$$

$$Pgrid_{i,x} := 8\cdot\sum_{n=1}^{i}\int_{0}^{n\cdot Sg_i}(Jm\cdot Sg_i\cdot y)^2\cdot\frac{\rho}{A_{g_x}}\,dy \qquad \%Em_i := \frac{100\cdot Pemit_i}{Pin\cdot Wc^2} \qquad \%Gr_{i,x} := \frac{100\cdot Pgrid_{i,x}}{Pin\cdot Wc^2} \qquad \%L_{i,x} := \%Sh_{i,x} + \%Gr_{i,x} + \%Em_i$$

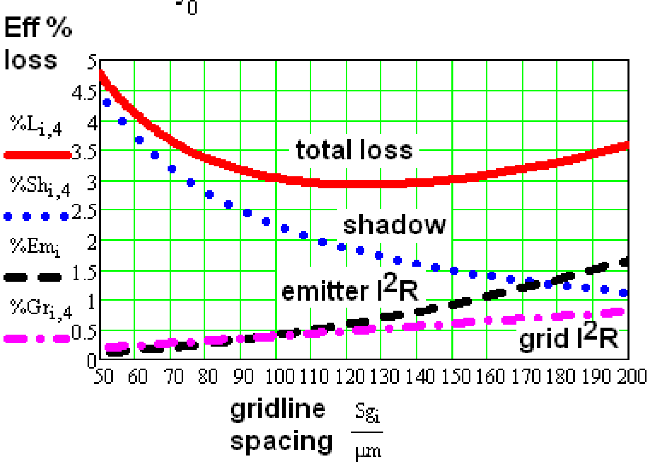

Choose optimum # (z) of gridlines per triangle

$z := 43 \qquad y := 2 \qquad Sg_z = 116.279\cdot\mu m$

$$\frac{8\cdot(d_y + 2\cdot dw)\cdot\left[\sum_{n=1}^{z}(n\cdot Sg_z) - \frac{Wc}{4}\right]}{Wc^2} = 0.029$$

Shadow

Grid I²R loss equiv R $\quad Rgr := \frac{Pgrid_{z,y}}{(Jm\cdot Wc^2)^2} = 0.0079\cdot\Omega$

Emitter I²R loss equiv R $\quad Rem := \frac{Pemit_z}{(Jm\cdot Wc^2)^2} = 0.0058\cdot\Omega$

$$Rs := Rgr + Rem = 0.014\cdot\Omega \qquad v := \frac{Voc}{n\cdot 0.026V} \qquad r := \frac{Voc}{Jm\cdot Wc^2} = 0.507\cdot\Omega \qquad rs := \frac{Rs}{r} \qquad FF := \frac{v - \ln(v+1)}{1+v}(1 - rs) = 0.865$$

Figure 9. MathCAD grid design optimization and series resistance Rs of grid and emitter for cell. Total Rs does not include tunnel junction here but it is included in Table 1.

4.3 General Overview of Bi-Facial Epigrowth and Cell Process

N-type 4in GaAs wafers were purchased “epi-ready” (on one side) and double-side polished. Wafer bow from the 2.5% lattice mismatched InGaAs bottom cell must be controlled. For small bow, we derive from Stoney’s formula: Bow = $\frac{3}{4} d^2 \varepsilon (M_F/M_S)(t_F/t_S^2)$ where ε is the strain, t_F is the film and t_S is the substrate (wafer) thickness, d is the wafer diameter, and M_F and M_S are the film and wafer biaxial elastic moduli. Since the InGaAs relaxes as dislocations are formed, the strain is much less than 2.5%. The formula reveals useful trends such as bow increases with the square of the wafer diameter or decreases with the square of wafer thickness. Wafers 625-650μm generally have no noticeable bow. Wafers as thin as 350μm could be and were processed (with bow on the order of 0.5mm).

The bi-facial cell substrate needs to be transparent to near-infrared light to illuminate the InGaAs cell. N-type GaAs wafers doped $\sim 10^{17}$ cm^{-3} are used. Free carrier absorption for N GaAs is over 10X less than for P-GaAs. The free carrier absorption coefficient is ~0.6 cm^{-1} for N GaAs for wavelengths between 1 to 2μm[12] and results in less than 4% QE loss for a 650μm wafer. Figure 10 shows measured transmission loss through a bare GaAs wafer and the calculated transmission using data from Palik[13]. This is uncoated material so there is ~28% Fresnel loss at these wavelengths from each interface leading to the ~50% transmission. The abrupt 890nm turn-on is not electron free-carrier loss (which varies slowly as λ^2) and is due to phonon-related optical transitions near the GaAs bandedge. The (100) wafers are cut 10^o to the 111A so that the InGaP top cell has a higher bandgap (~1.89eV) than if less tilt was used[14].

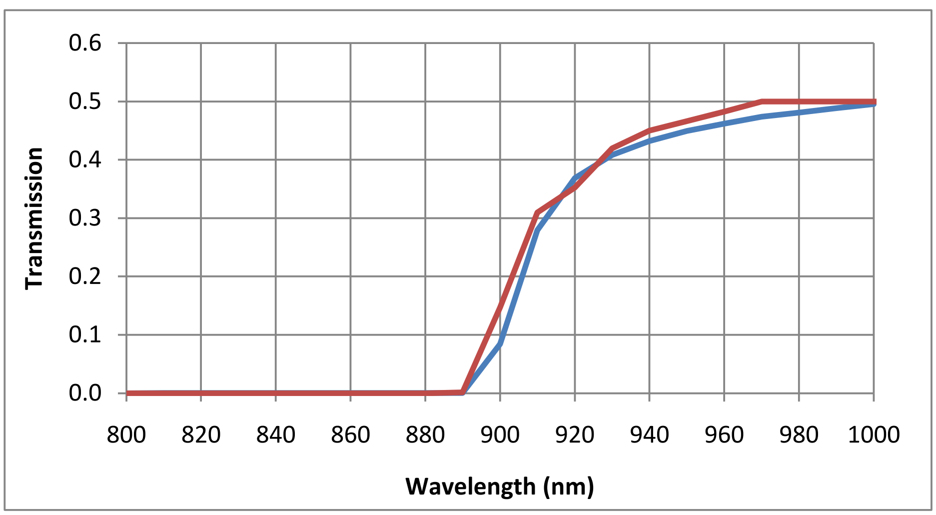

Figure 10. Measured (blue) vs. theory (red) transmission loss through bare 350μm GaAs wafer.

An InAlGaAs grading layer is grown first on the non-“epi-ready” side on the GaAs wafer followed by the lattice mismatched 0.94eV N/P InGaAs cell. Defects from growth on the non-epi-ready backside are unlikely to affect the 2.5% lattice mismatched InGaAs cell material which will have 10^6-$10^7/cm^2$ dislocations. After bottom cell growth, the wafers are unloaded into a cassette, run through and rinse/spin dryer to remove particles, and are then flipped and reloaded into the in the MOCVD reactor.

A tunnel junction, a 1.42eV GaAs middle cell, a tunnel junction, and the final 1.89eV InGaP cell are grown lattice matched on the opposite (epi-ready) GaAs wafer surface (Table 2). If InGaP-type grades are used on the cell backside, or if the middle GaAs and upper InGaP cells are grown first, the phosphine degrades the opposite GaAs wafer surface so that additional processing (e.g. lapping) or protection of that surface would be needed.

Table 2. Epistructure of NREL-Verified 41% (eft, D09) vs 42.2% (right, D11) 500X Concentrator Cells

Best cell 1xJsc; Voc; FF	41% 500X D09 L810-952-3-951-3 13.6mA/cm^2; 3.495V; 0.851	Thickness nm	Doping cm^{-3}	42.2% 500X D11 L873-1141-6-1140-1 14.1mA/cm^2; 3.468V; 0.866	Thickness nm	Doping cm^{-3}	
contact cap	N GaAs	60	>1e19	N GaAs	60	>1e19	Te
spacer	N GaAs	200	2.0E+18	N GaAs	200	2.0E+18	Si
window	N $InAl_{0.5}P_{0.5}$	20	8.0E+18	**N $InAl_{0.6}P_{0.4}$**	20	8.0E+18	Si
emitter	N $In_{0.49}Ga_{0.51}P$	60	1e18 to 8e18	N $In_{0.49}Ga_{0.51}P$	60	1e18 to 8e18	Si
base	P $In_{0.49}Ga_{0.51}P$	1200	3.0E+16	P $In_{0.49}Ga_{0.51}P$	**1400**	3.0E+16	Zn
BSF	P $In_{0.49}(Al_{0.3}Ga_{0.7})_{0.51}P$	100	8.0E+17	P $In_{0.49}(Al_{0.3}Ga_{0.7})_{0.51}P$	100	8.0E+17	Zn
TJ1	P $Al_{0.4}Ga_{0.4}As$	100	1.0E+20	P $Al_{0.4}Ga_{0.4}As$	100	1.0E+20	C
TJ1	N GaAs	25	1.4E+19	N GaAs	**20**	1.4E+19	Te
window	N $Al_{0.4}Ga_{0.4}As$	30	1.0E+18	N $Al_{0.4}Ga_{0.4}As$	30	1.0E+18	Si
emitter	N GaAs	85	1.0E+18	N GaAs	**100**	1.0E+18	Si
base	P GaAs	3500	2.0E+17	P GaAs	**4000**	2.0E+17	Zn
absorber				**p+-In0.01GaAs**	**500**	**2e17 to 2e18**	Zn
BSF	P $Al_{0.3}Ga_{0.7}As$	150	1.0E+18	P $Al_{0.3}Ga_{0.7}As$	150	1.0E+18	Zn
TJ2	P $Al_{0.4}Ga_{0.4}As$	100	1.0E+20	P $Al_{0.4}Ga_{0.4}As$	100	1.0E+20	Zn
TJ2	N GaAs	30	1.4E+19	N GaAs	30	1.4E+19	Si
buffer	N GaAs	200	2.0E+18	N GaAs	200	2.0E+18	Si
wafer	N GaAs (4in WAF410)	650μm	1.0E+17	N GaAs (4in WAF410)	650μm	1.0E+17	Si
buffer	N GaAs	150	2.0E+18	N GaAs	150	2.0E+18	Si
grade 1	N $In_{0.03}(Al_{0.6}Ga_{0.4})_{0.97}As$	250	4.0E+17	N $In_{0.03}(Al_{0.6}Ga_{0.4})_{0.97}As$	250	4.0E+17	Si
grade 2	N $In_{0.07}(Al_{0.6}Ga_{0.4})_{0.93}As$	250	4.0E+17	N $In_{0.07}(Al_{0.6}Ga_{0.4})_{0.93}As$	250	4.0E+17	Si
grade 3	N $In_{0.10}(Al_{0.6}Ga_{0.4})_{0.90}As$	250	4.0E+17	N $In_{0.10}(Al_{0.6}Ga_{0.4})_{0.90}As$	250	4.0E+17	Si
grade 4	N $In_{0.14}(Al_{0.6}Ga_{0.4})_{0.86}As$	250	4.0E+17	N $In_{0.14}(Al_{0.6}Ga_{0.4})_{0.86}As$	250	4.0E+17	Si
grade 5	N $In_{0.17}(Al_{0.6}Ga_{0.4})_{0.83}As$	250	4.0E+17	N $In_{0.17}(Al_{0.6}Ga_{0.4})_{0.83}As$	250	4.0E+17	Si
grade 6	N $In_{0.21}(Al_{0.6}Ga_{0.4})_{0.79}As$	250	4.0E+17	N $In_{0.21}(Al_{0.6}Ga_{0.4})_{0.79}As$	250	4.0E+17	Si
grade 7	N $In_{0.24}(Al_{0.6}Ga_{0.4})_{0.76}As$	250	4.0E+17	N $In_{0.24}(Al_{0.6}Ga_{0.4})_{0.76}As$	250	4.0E+17	Si
grade 8	N $In_{0.28}(Al_{0.6}Ga_{0.4})_{0.72}As$	250	4.0E+17	N $In_{0.28}(Al_{0.6}Ga_{0.4})_{0.72}As$	250	4.0E+17	Si
grade 9	N $In_{0.31}(Al_{0.6}Ga_{0.4})_{0.69}As$	250	4.0E+17	N $In_{0.31}(Al_{0.6}Ga_{0.4})_{0.69}As$	250	4.0E+17	Si
gr10/window	N $In_{0.36}(Al_{0.6}Ga_{0.4})_{0.64}As$	450	5.0E+17	N $In_{0.36}(Al_{0.6}Ga_{0.4})_{0.64}As$	**450**	5.0E+17	Si
emitter	N $In_{0.35}Ga_{0.65}As$	300	5.0E+17	N $In_{0.35}Ga_{0.65}As$	300	5.0E+17	Si
base	P $In_{0.35}Ga_{0.65}As$	1700	6.0E+16	P $In_{0.35}Ga_{0.65}As$	1700	**6e16 to 4e17**	Zn
BSF	P $In_{0.36}(Al_{0.6}Ga_{0.4})_{0.64}As$	100	5.0E+17	P $In_{0.36}(Al_{0.6}Ga_{0.4})_{0.64}As$	100	5.0E+17	Zn
contact cap	P $In_{0.35}Ga_{0.65}As$	600	2.0E+19	P $In_{0.35}Ga_{0.65}As$	**400**	2.0E+19	Zn

The wafers were epitaxially grown in a Veeco (Emcore) E450 low pressure MOCVD reactor which can load thirteen 4in wafers per run. For these growths the hydrogen mainflow was 120slpm and pressure was 50torr. Metal-organics used were TMIn, TMGa, TMAl and hydrides were 100% arsine and phosphine. Dopant sources were a DMZn bubbler for P-type and silane for N-type cell material. Tunnel junctions (TJs) and N GaAs caps used CBr_4 and DeTe. Growth temperature and V/III ratios were ~60/660C for InGaP, 30/600C for GaAs, and 60/600C for In(Al)GaAs, respectively. Growth rates were ~8A/s for InGaP, 20A/s for GaAs, and 10A/s for InGaAs. Conditions for tunnel junctions differ and are proprietary.

The cell process after epigrowth is relatively simple and the main steps are outlined here. The backside 600nm thick InGaAs cap is wet etched to remove a layer of InGaAs "damaged" by phosphine from the final InGaP growth. CrNiAu is evaporated over the entire wafer backside and acts as a back contact for the cell and optical mirror. The Cr sticking layer and Ni solder barrier are made thin since they are poor infrared reflectors.

New positive resist is applied and openings are made for the gridlines in an amine image reversal process used to make dovetails for clean metal liftoff. The evaporated gridlines of the high efficiency cells reported here are 4-5μm of TiPtAu as shown earlier in Figure 7.

A second photolithography step is used to define areas over the busbars where the AR coating will be removed by liftoff. The GaAs cap is then stripped in a citric-based etch selective against the InAlP window. A double layer 120nm MgF_2/ 60nm ZnS antireflection coating is evaporated (for cells without coverglass) and the AR film over the busbars is lifted off in acetone.

The wafer fronts are protected with resist, mounted on tape, and then diced. The dicing is the last fabrication step and defines the cell junction area.

4.4 1.9eV InGaP Top Subcell Development

Table 3 shows the epistructure and illuminated IV data of the final single junction InGaP subcell closest to that used in the final tandems. A tunnel junction is included so this N/P InGaP top subcell was grown on the same lightly doped N GaAs wafers as used for the tandems.

Table 3. Epistructure of Single Junction InGaP Developmental Subcell

	Epi ID: m2-1115	Temp	V/III	Bandgap	Thickness	Doping	Comments
	Cell Lot: L864	C	ratio	eV	nm	cm^{-3}	
cap	n+-GaAs	600	30	1.42	60	Te, >1e19	heavy doping for non-alloyed TiPtAu ohmic contact
spacer	n-GaAs	600	30	1.42	200	Si, 2e18	spacer improves Voc and Jsc
window	n-$In_{0.4}Al_{0.6}P$	660	60	2.23 (x)	20	Si, 8e18	LMM pseudomorphic, shifts cut-on λ 10nm vs LM
emitter	n-$In_{0.49}Ga_{0.51}P$	660	60	1.88	60	Si, 1 to 8e18	graded emitter improves Jsc, Rsh 500Ω/sq
base	p-$In_{0.49}Ga_{0.51}P$	660	60	1.88	1200	Zn, 3e16	changed to 1.4um in final tandems to add 0.2mA to Jsc
BSF	p-$In_{0.49}(Al_{0.3}Ga_{0.7})_{0.51}P$	660	60	2.0 (x)	100	Zn, 8e17	maximum Zn doping possible
TJ1	p+-$Al_{0.4}Ga_{0.6}As$			1.92	100	C, 1e20	lower temp and V/III ratio (proprietary)
TJ2	n+-GaAs			1.42	30	Te, 1.4e19	lower temp and flushes (proprietary)
buffer	n-GaAs	600	30	1.42	200	Si, 2e18	
wafer	100 GaAs cut 10^{o} to 111A			1.42	650μm	Si, 1e17	offcut helps give higher disordered LM InGaP bandgap
						Wafer	1xJsc 14.01mA/cm^2 1xVoc 1.408V 1xFF 0.881
						Averages	At 492 suns: Voc 1.615V FF 0.808

In order to increase the 1xJsc by 0.2mA/cm^2 to reach the roadmap (Table 1) level, we made the base slightly (0.2µm) thicker in the final tandems. The added thickness was based on calculations using published lattice matched $In_{0.49}Ga_{0.51}P$ n and k optical constant data from Ferrini[15]. Separately, Dean Levi[16] and Sarah Kurtz[17] of NREL also supplied data. All data was found to be in close agreement (Figure 11). Figure 12 shows the expected 1xJsc variation.

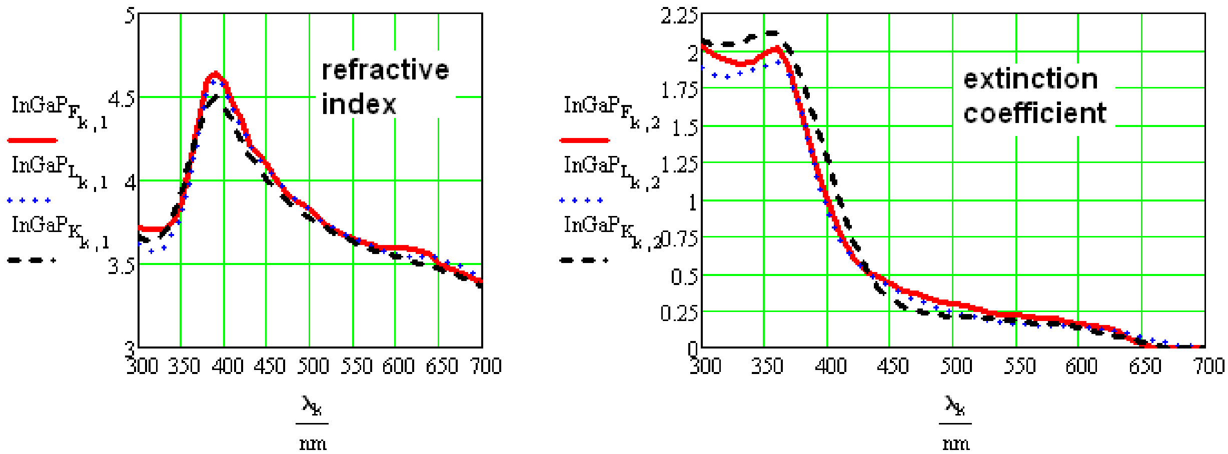

Figure 11. Optical constants for $In_{0.49}Ga_{0.51}P$ from Ferrini (F), Levi (L) and Kurtz (K).

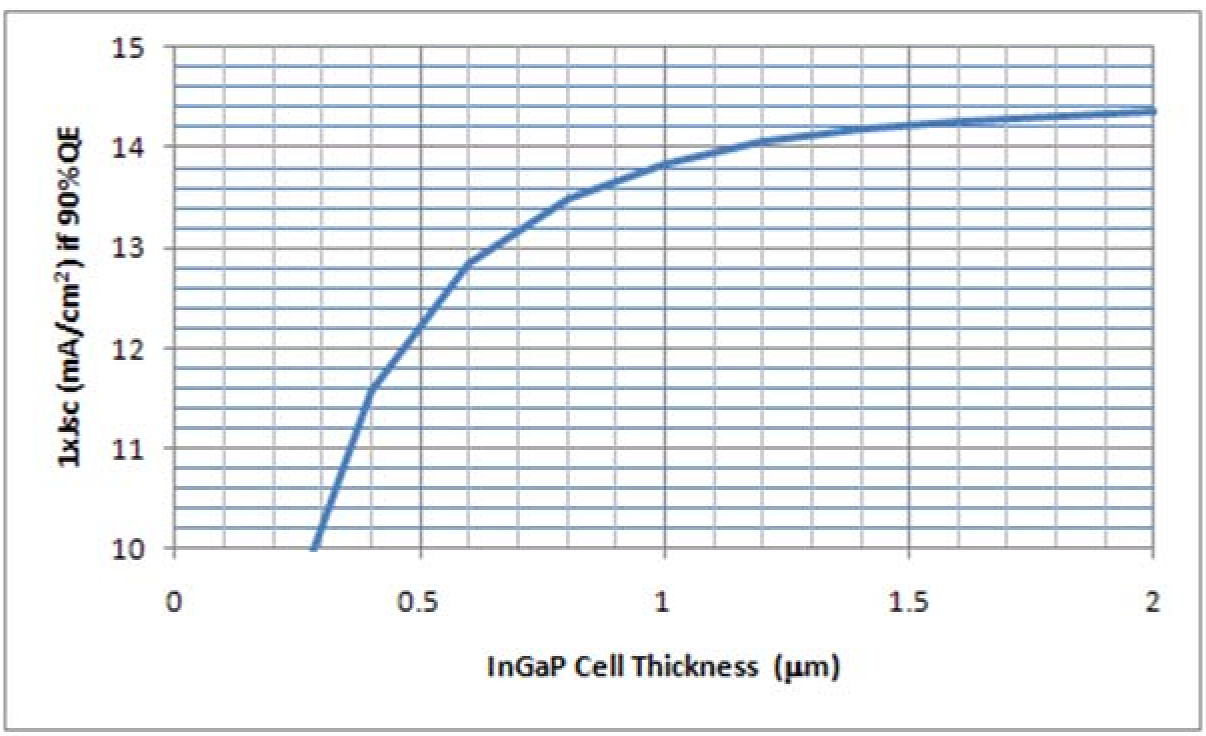

Figure 12. Calculated 1xJsc (AM1.5D, 100mW/cm^2) vs. total $In_{0.49}Ga_{0.51}P$ cell thickness.

Figure 12 indicated adding 0.2µm to the base should increase the 1xJsc by 0.2mA/cm^2 in the final delivered program cells. Of course, this will leave the GaAs middle cell with 0.2mA less, but the optimization took this into account so that the expected Jsc for all subcells is in excess of 14.2mA/cm^2 in the final design.

In order to optimize design of the InAlP window used in the InGaP top cell, good data on the absorption in the InAlP window was also needed. J.A. Woollam provided the InAlP spectroscopic data (Figure 13). A significant amount of the light absorbed in the InAlP window is lost to recombination, but not all. In the roadmap (Table 1), we estimate this loss as 50% of the indicated Jsc absorption value in Fig. 13, based on the hand-waving argument that half the photogenerated carriers will diffuse upwards towards the cell surface and be lost to surface recombination, and that the other half will move towards and fall down the potential hill at the emitter and be collected. The window is so thin (20nm) that hole diffusion length in the N InAlP may not be a major issue since most likely it is well in excess of 20nm.

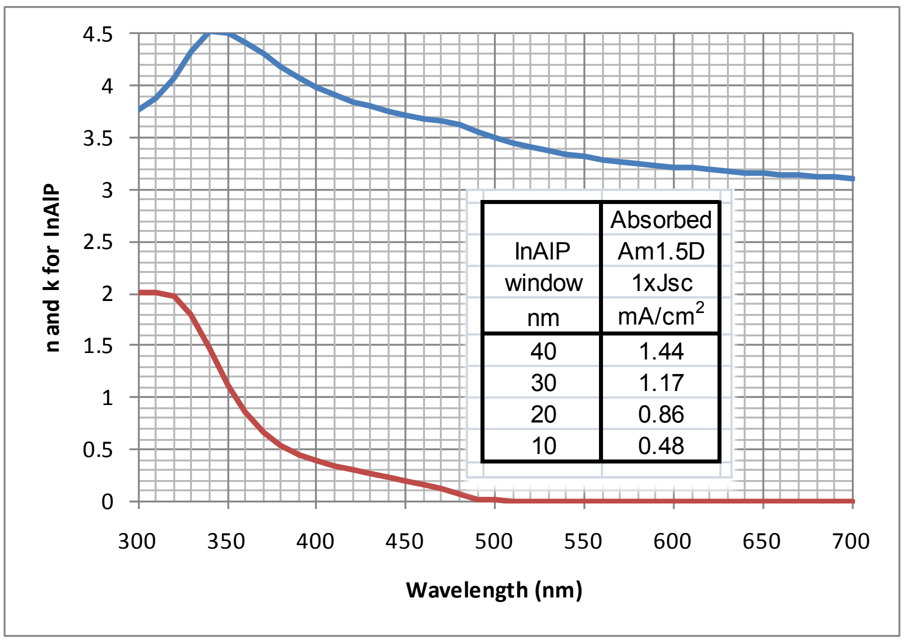

Figure 13. Spectroscopic ellipsometry data for $In_{0.5}Al_{0.5}P$ on 10° cut GaAs wafers.

4.5 GaAs Middle Cell Development

Although not a task explicitly called out in the original program SOW because of the advanced state of GaAs cell technology, we did examine single junction GaAs middle cells to help us interpret the tandem cell performance. Two types of GaAs cells were employed in the program. A standard N/P GaAs cell was in use for all of the program, until the final delivery.

We needed to increase the 1xJsc of the middle cell to make progress with the tandem. We wanted to increase the InGaP thickness from 1.2 to 1.4µm to increase the top cell Jsc, but this would deprive the GaAs cell of ~0.2mA/cm^2. We needed to compensate for this Jsc loss and add more so that the middle cell would also have 14.2mA/cm^2 under the new InGaP top cell.

4.5.1 Bandgap Narrowing to Extend Cutoff

We noticed the GaAs cells always had QE in excess of 872nm, the cutoff expected for 1.424eV GaAs, whether measured by NREL or Spire. We assumed that this "below-bandgap" response was possible through bandgap narrowing in doped GaAs. We increased the doping in the base and examined the results (Figure 14). Although there was a 0.12mA increase in Jsc in the below bandgap QE, the additional shift of the cutoff wavelength was compensated by the lower diffusion length due to the heavier doping at shorter wavelengths and therefore was useless.

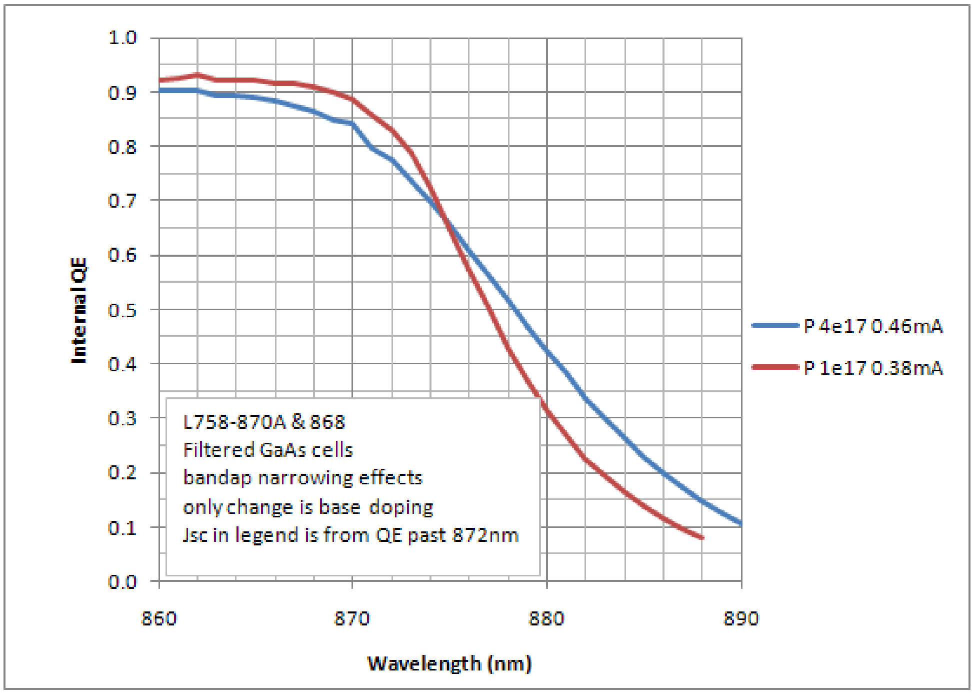

Figure 14. Increase of long wavelength QE through bandgap narrowing in GaAs base.

4.5.2 Pseudomorphic Absorption Layer to Extend Cutoff

Next, we thought about lowering the bandgap by compositional change. InGaP/GaAs/Ge cells add 1% indium to the GaAs to lattice match with the Ge substrate. We did not wish to make a thick lattice-mismatched cell mainly because we worried that the tunnel junction dopants would diffuse more in such a structure. Instead, we tried to add a pseudomorphic thin 1%InGaAs layer at the back of the GaAs cell to boost the long wavelength QE. 1% InGaAs has a bandgap of 1.415eV and a cutoff of 876nm. Since the AM1.5D spectral slice from 870 to 880nm can add 0.7mA/cm^2 in just that 10nm, we reasoned that the 4nm 872 to 876nm shift could add 0.28mA/cm^2, on the order of the increase needed. In addition, since the bandgap shift was only 9meV, less than the thermal kT energy of carriers at 26meV, we reasoned there should be no significant barrier for collection at the interface. The 1% InGaAs represents a 717ppm mismatch to GaAs. The critical thickness (at which it is energetically favorable to generate dislocations to relieve stress instead of continuing elastic accommodation) is calculated using the Mathews-Blakeslee[18] theory in Figure 15 as 0.5µm for 1% (0.01) indium added to the GaAs.

Critical thickness of In(x)Ga(1-x)As on GaAs $\quad ang := 10^{-10} \cdot m \quad q := 1.6 \cdot 10^{-19} \cdot C \quad eV := q \cdot V$

$GaAs := 5.653ang \quad InAs := 6.0583ang \quad x := 0, 0.001 .. 0.05 \quad ppm := 10^{-6}$

$InGaAs(x) := (InAs - GaAs) \cdot x + GaAs$

$mismatch(x) := \dfrac{|InGaAs(x) - GaAs|}{GaAs} \quad mismatch(0.01) = 716.964ppm$ mismatch for 1% indium

$b(x) := \dfrac{InGaAs(x)}{\sqrt{2}}$ typical Burgers vector for (100) $\quad Eg(x) := \left(1.424 - 1.562 \cdot x + 0.494 \cdot x^2\right) \cdot eV$

$\upsilon := 0.3$ typical Poisson ratio

$\lambda := 60deg$ angle between slip direction and line in interface plane normal to line of intersection between slip plane and interface

$\theta := 60deg$ angle between dislocation line and Burgers vector (abt 60 deg)

$$h(x) := root\left[\left[\frac{b(x) \cdot \left(1 - \upsilon \cdot \cos(\theta)^2\right)}{4 \cdot \pi \cdot (1 + \upsilon) \cdot \cos(\lambda) \cdot mismatch(x)} \cdot \left(\ln\left(\frac{z}{b(x)}\right) + 1\right) - z\right], z, 10ang, 10\mu m\right]$$ critical thickness

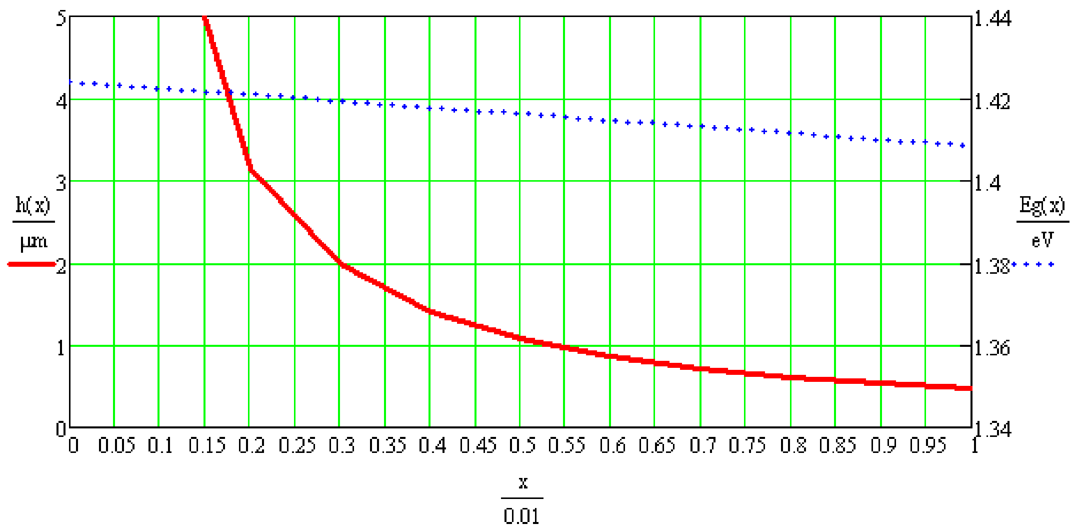

Figure 15. Critical thickness calculation for $In_xGa_{1-x}As$ on GaAs (1 on X-axis → 1%).

We wanted to grow this 1%InGaAs absorbing layer as thick as possible to maximize its optical absorption, but yet keep it below its critical thickness. Table 4 shows a comparison of the standard GaAs middle cell with the "pseudomorphic" structure used in the final delivery. The final subcell (L843-1051) achieved the 14.2mA/cm^2 goal. However, the wafer surface of the final tandem epigrowths exhibited a slight cross-hatch (Figure 16). Despite adhering to the theory, there was some relaxation (the 1%InGaAs long wavelength absorbing layer was NOT pseudomorphic). Surfaces without the 1%InGaAs layer are smooth and featureless. However, since the Voc was still acceptable and the tunnel junctions (TJs) worked at the 500X level (the TJ dopants did not diffuse disastrously due to the dislocations), this middle cell was selected.

Table 4. Epistructure of Single Junction InGaP Developmental Subcell

Single Junction Test Cells All Process L843 (same AR coat)	m2-1007 Filtered GaAs Middle cell **3.5um base**			m2-1048 Filtered GaAs Middle cell **4.5um base**			m2-1051 Filtered GaAs Middle cell **4um base +0.5um 1%InGaAs**		
	material	Thick. nm	Doping cm^{-3}	material	Thick. nm	Doping cm^{-3}	material	Thick. nm	Doping cm^{-3}
contact cap	p+-GaAs	250	>1e19	p+-GaAs	250	>1e19	p+-GaAs	250	>1e19
top cell filter	p-InGaP	1260	1.0E+18	p-InGaP	1260	1.0E+18	p-InGaP	1260	1.0E+18
TJ1	p+-Al0.4GaAs	100	1.0E+20	p+-Al0.4GaAs	100	1.0E+20	p+-Al0.4GaAs	100	1.0E+20
TJ1	n+-GaAs	20	1.4E+19	n+-GaAs	20	1.4E+19	n+-GaAs	20	1.4E+19
window	n-Al0.4GaAs	30	1.0E+18	n-Al0.4GaAs	30	1.0E+18	n-Al0.4GaAs	30	1.0E+18
emitter	n-GaAs	85	1.0E+18	n-GaAs	100	1.0E+18	n-GaAs	100	1.0E+18
base	p-GaAs	**3500**	2.0E+17	p-GaAs	**4500**	2.0E+17	p-GaAs	**4000**	2.0E+17
LW absorber							**p+-In0.01GaAs**	500	2e17 to 2e18
BSF	p-Al0.3GaAs	150	1.0E+18	p-Al0.3GaAs	150	1.0E+18	p-Al0.3GaAs	150	1.0E+18
TJ2	p+-Al0.4GaAs	100	1.0E+20	p+-Al0.4GaAs	100	1.0E+20	p+-Al0.4GaAs	100	1.0E+20
TJ2	n+-GaAs	30	1.4E+19	n+-GaAs	30	1.4E+19	n+-GaAs	30	1.4E+19
buffer	n-GaAs	200	2.0E+18	n-GaAs	200	2.0E+18	n-GaAs	200	2.0E+18
wafer	GaAs		1.0E+17	GaAs		1.0E+17	GaAs		1.0E+17
Wafer Avg (52 cells):									
1xJsc (mA/cm^2)	13.81			13.98			14.20		
1xVoc (V)	1.000			0.997			0.995		
1xFF	0.864			0.863			0.866		
Suns	490			na			492		
Voc (V)	1.184			na			1.181		
FF**	0.687			na			0.686		
**thin grid metal									

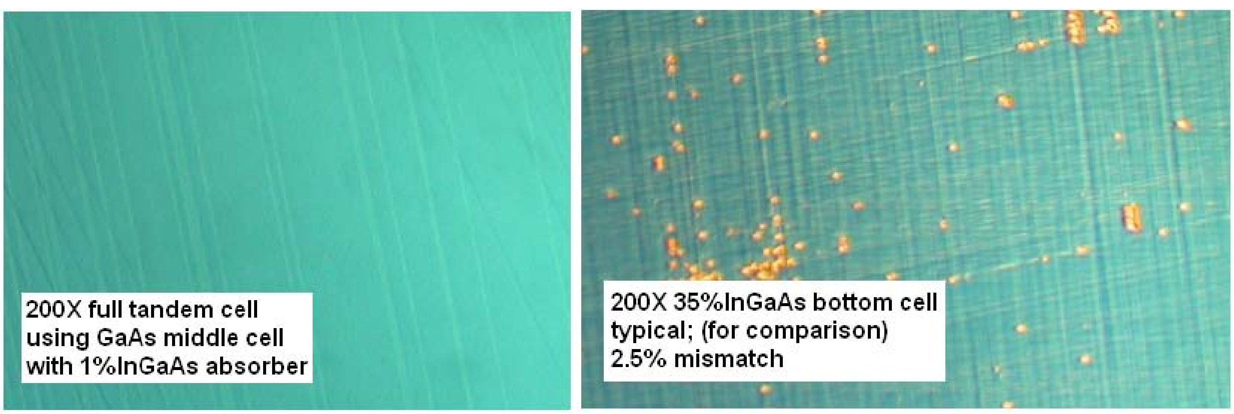

Figure 16. Left: Crosshatch on top and middle cell surface vs Right: Bottom cell. Credit: Spire.

4.6 Tunnel Junction Development

There are two tunnel junctions (TJs) in the tandem (Fig. 17). For 500X operation (i.e. ~7A/cm2) , we found carbon doped P AlGaAs and Te-doped N GaAs were usable. One TJ is between the top and middle cells. The N GaAs thickness in the upper TJ needs to be thin to limit absorption of light that could be used by the GaAs cell. The second TJ is under the GaAs middle cell since we need to use an N GaAs wafer under the N/P GaAs cell to limit free carrier absorption of infrared photons for the bottom cell.

This lower TJ does not need to be thin since few absorbable photons are left after the GaAs cell, and the GaAs wafer would absorb them anyway. IV data of stand-alone TJs using the same

AlGaAs P layer but 20nm GaAs N layer (upper TJ) and 30nm GaAs N layer (lower TJ) are shown in Table 5. Both TJs have a layer grown on top of them to simulate the heat and duration that would occur in a tandem. The sum of the Rs of the two TJs is used in the Table 1 roadmap.

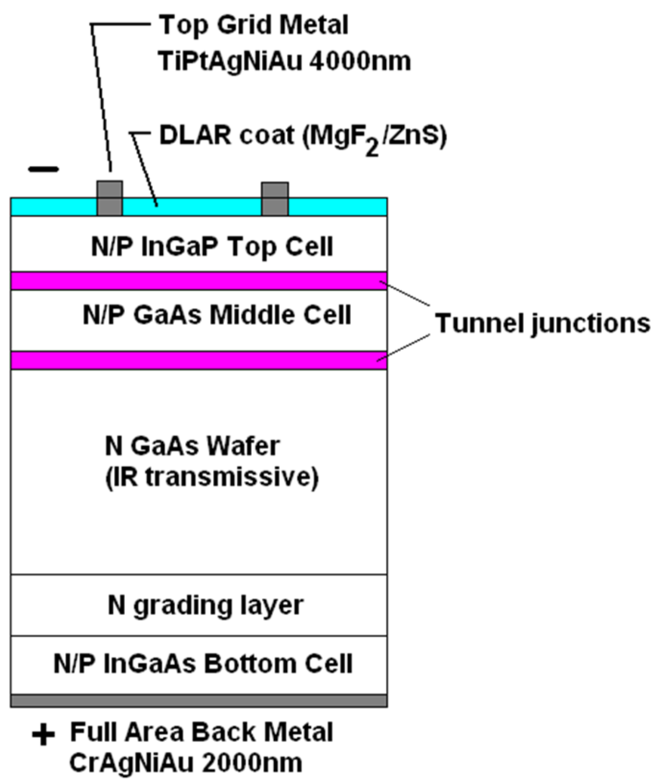

Figure 17. TJ position in bi-facial tandem.

Table 5. Data on Upper and Lower TJs in Tandem

ID	GaAs TJ nm	Post TJ anneal	Test	Rs $m\Omega\text{-}cm^2$	Jp A/cm^2
L844-1058	20	1.3um GaAs 660C	diode 1	2.64	30.2
upper TJ1		growth rate to	diode 2	2.64	37.5
		match InGaP	diode 3	2.22	46.5
			average	2.50	38.1
L707-730	30	1.5um InGaP 660C	diode 1	0.59	172
lower TJ2			diode 2	0.48	168
			average	0.53	170

Figure 18 shows typical IVs of the tunnel junctions for which data is summarized in Table 5. In tandem cell operation, the TJs are forward biased (operate to the right in positive bias). The peak current for a 500X tandem (about $7A/cm^2$) is exceeded by both TJs, and the data indicate the current TJs should be useful well past 1500X. Figure 19 is a plot of the equivalent Jsc loss for the GaAs cell vs GaAs N layer TJ thickness integrated between 660 and 880nm.

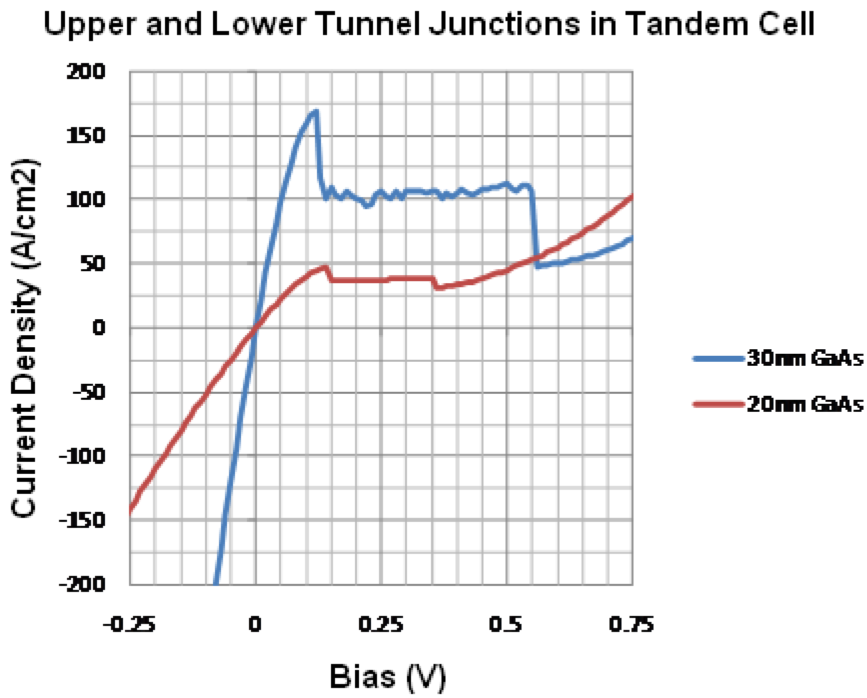

Figure 18. Typical TJ IVs from data in Table 6.

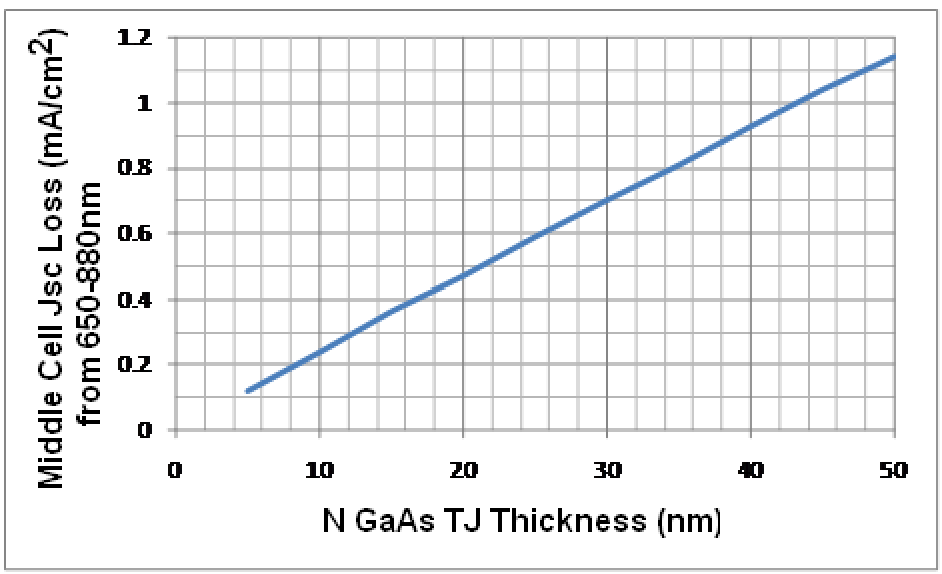

Figure 19. Jsc loss vs N GaAs layer thickness in upper TJ.

Finally, Figure 20 shows a rough calculation of the "small signal" (before Jpeak) TJ resistance adapted from Wang[19]. The plot demonstrates how quickly the resistance can vary with doping (through change of the depletion width/tunnel barrier). The calculated values of 1-2mΩ-cm^2 roughly agree with the measured data reported above.

P AlGaAs/N GaAs Tunnel Junction Contact Resistance Estimate

$q := 1.602 \cdot 10^{-19} \cdot C$ $\quad h := 6.626 \cdot 10^{-34} \cdot J \cdot s$ $\quad m_o := 9.1 \cdot 10^{-31} \cdot kg$ $\quad eV := q \cdot V$ $\quad \varepsilon o := 8.85 \cdot 10^{-14} \cdot \frac{F}{cm}$ $\quad k := 1.38 \cdot 10^{-23} \cdot \frac{J}{K}$

$Tj := 300K$ $\quad m_e := 0.07$ $\quad m_{hh} := 0.55$ $\quad \varepsilon r := 13.1$ $\quad Eg := 1.42 \cdot eV$ $\quad Na := 1.4 \cdot 10^{19} \cdot cm^{-3}$

$$n_i := \sqrt{2 \cdot \left(\frac{2 \cdot \pi \cdot m_e \cdot m_o \cdot k \cdot Tj}{h^2}\right)^{1.5}} \cdot \sqrt{2 \cdot \left(\frac{2 \cdot \pi \cdot m_{hh} \cdot m_o \cdot k \cdot Tj}{h^2}\right)^{1.5}} \cdot \exp\left(\frac{-Eg}{2 \cdot k \cdot Tj}\right) = 2.546 \times 10^{6} \cdot cm^{-3}$$

$Mr := \frac{m_e \cdot m_{hh} \cdot m_o}{m_e + m_{hh}}$ $\quad \varepsilon s := \varepsilon r \cdot \varepsilon o$ $\quad i := 0 .. 100$ $\quad Nd_i := 10^{18 + \frac{i}{50}} \cdot cm^{-3}$ $\quad Vd_i := \frac{k \cdot Tj}{q} \cdot \ln\left(\frac{Na \cdot Nd_i}{n_i^2}\right)$

$Wd_i := \sqrt{\frac{2 \cdot \varepsilon s \cdot Vd_i \cdot (Na + Nd_i)}{q \cdot Na \cdot Nd_i}}$ $\quad E_i := \frac{Vd_i}{\frac{Wd_i}{2}}$ $\quad Eo_i := \frac{q \cdot h \cdot E_i}{2 \cdot \pi^2 \cdot \sqrt{2 \cdot Mr \cdot Eg}}$ $\quad R_{TJ_i} := \frac{h^3}{4 \cdot \pi \cdot q^2 \cdot Mr \cdot Eo_i \cdot \exp\left(\frac{-\pi^2 \cdot \sqrt{Mr} \cdot Eg^{1.5}}{\sqrt{2} \cdot q \cdot h \cdot E_i}\right)}$

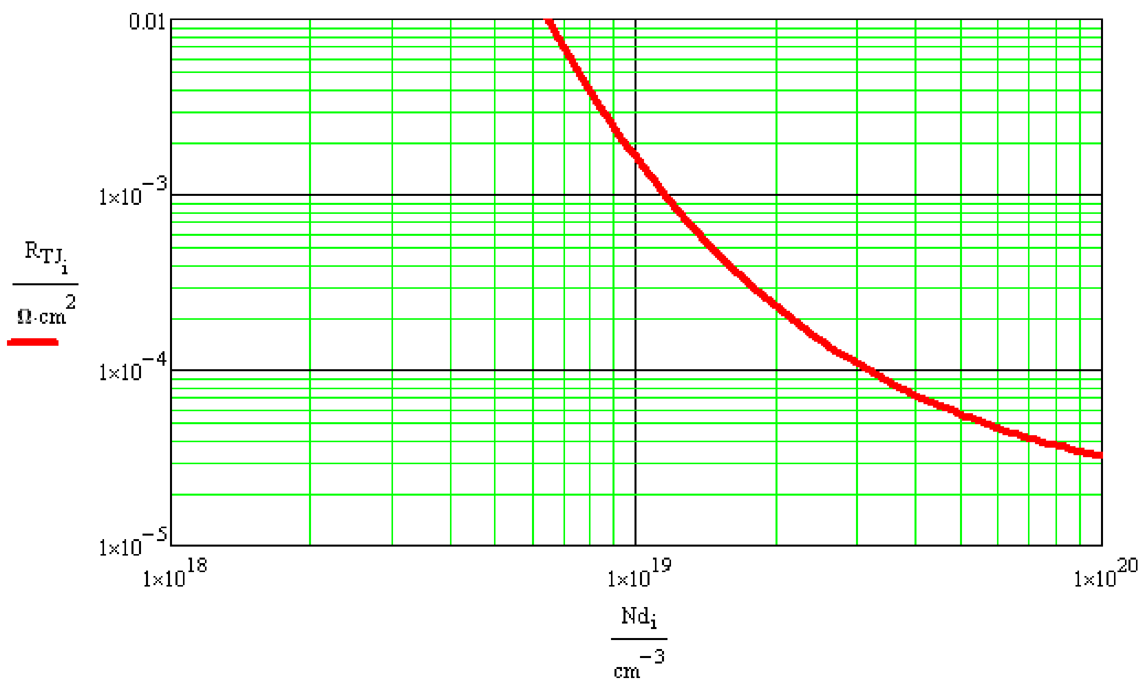

Figure 20 Rough calculation of TJ resistance for P AlGaAs/N GaAs (dominated by GaAs).

4.7 Lattice Mismatched InGaAs Bottom Cell Development

Growth of the InGaAs bottom cell was described in Section 4.3. We discovered that the most manufacturable growth sequence was to grow an InAlGaAs grading layer first on the back of the wafer followed by an InGaAs bottom cell. In this way, the opposite wafer surface is preserved for growth. If an InGaP grading layer is used, the opposite wafer surface is severely degraded. A SiN layer could be deposited and then removed to protect this surface, but this entails significant added processing (a time-consuming PECVD SiN deposition and subsequent wet etch). If the GaAs middle and InGaP top cells are grown first, the opposite wafer side is again degraded by the InGaP growth and the back surface must either be protected or lapped.

4.7.1 InGaAs Cell Composition (Cutoff Wavelength)

Figure 21 shows a calculation of the 1xJsc that InGaAs bottom cells of various cutoff wavelengths could generate. The 1330nm cutoff (about 35%InGaAs) is adequate for our roadmap (Table 1) and is at the edge of a absorption peak in the AM1.5D spectrum so that extending the cutoff a bit further will not result in significant additional Jsc.

Jsc from AM1.5D spectrum vs GaAs-filtered InGaAs cutoff wavelength assuming average 75% ext. QE

$q := 1.6\cdot10^{-19}\cdot C \quad h := 6.626\cdot10^{-34}\cdot J\cdot s \quad \eta := 0.75$

PS :=

	0	1
0	280	0
1	280.5	...

File with wavelength in nm and power spectrum in W/µm/m2

$i := 0..2000$

$\lambda_i := PS_{i,0}\cdot nm \qquad P_i := \frac{10}{9}\cdot PS_{i,1}\cdot\frac{W}{nm\cdot m^2}$ normalize from 90 to 100mW/cm²

$\lambda_{730} = 890\cdot nm \qquad k := 730..1800 \qquad Jsc_k := \frac{q\cdot\eta}{h\cdot c}\cdot\left[\sum_{j=730}^{k}\left[P_j\cdot\lambda_j\cdot\left(\lambda_{j+1}-\lambda_j\right)\right]\right]$

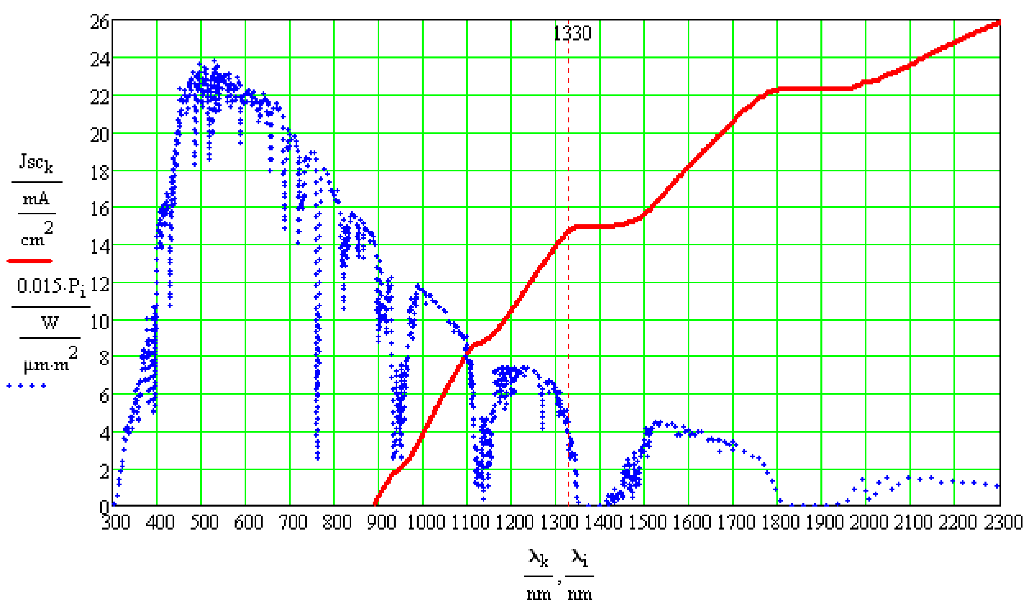

Figure 21. 1xJsc available from InGaAs cells of the indicated cutoff wavelength.

4.7.2 General $In_XGa_{1-X}As$ Absorption Model

In order to design the InGaAs bottom cell, absorption data was needed to estimate a suitable cell thickness. The data used a simple standard absorption model[20] and is compared with measured $In_{0.53}Ga_{0.47}As$ data (from J.A. Woollam) for model verification in Figure 22.

Physical Constants $h := 6.626 \cdot 10^{-34} \cdot J \cdot s$ $\quad \varepsilon_o := 8.85 \cdot 10^{-14} \cdot \frac{F}{cm}$ $\quad q := 1.6 \cdot 10^{-19} \cdot C$ $\quad eV := q \cdot V$ $\quad m_o := 9.1 \cdot 10^{-31} \cdot kg$

$i := 0..200 \qquad \lambda_i := 300nm + i \cdot 10nm \qquad x := 0..100$

$m_{e_x} := (0.063 - 0.023) \cdot \frac{x}{100} + 0.023 \qquad m_{h_x} := (0.51 - 0.41) \cdot \frac{x}{100} + 0.41 \qquad m_{r_x} := \frac{m_{e_x} \cdot m_{h_x}}{m_{e_x} + m_{h_x}}$

$n_{op} := 4$
average refractive index

$Eg_x := \left[1.424 - 1.562 \cdot \frac{x}{100} + 0.494 \cdot \left(\frac{x}{100}\right)^2\right] \cdot eV$

Dipole transition (Kane) energy - average of GaAs 22.71eV and InAs 21.1eV $\quad Ep := 21.8eV$

InGaAs53 :=

	0	1	2	3
0	300	3.61	2.25	$9.41 \cdot 10^5$
1	310	3.53	2.06	...

$$K_{abs_{i,x}} := \frac{q^2 \cdot \frac{2 \cdot \pi}{3} \cdot \frac{1}{(Eg_x)^2} \cdot \frac{Ep}{m_o} \cdot (2 \cdot m_{r_x} \cdot m_o)^{\frac{3}{2}}}{\lambda_i \cdot \varepsilon_o \cdot n_{op} \cdot h} \qquad \alpha_{i,x} := K_{abs_{i,x}} \cdot \sqrt{\frac{h \cdot c}{\lambda_i} - Eg_x}$$

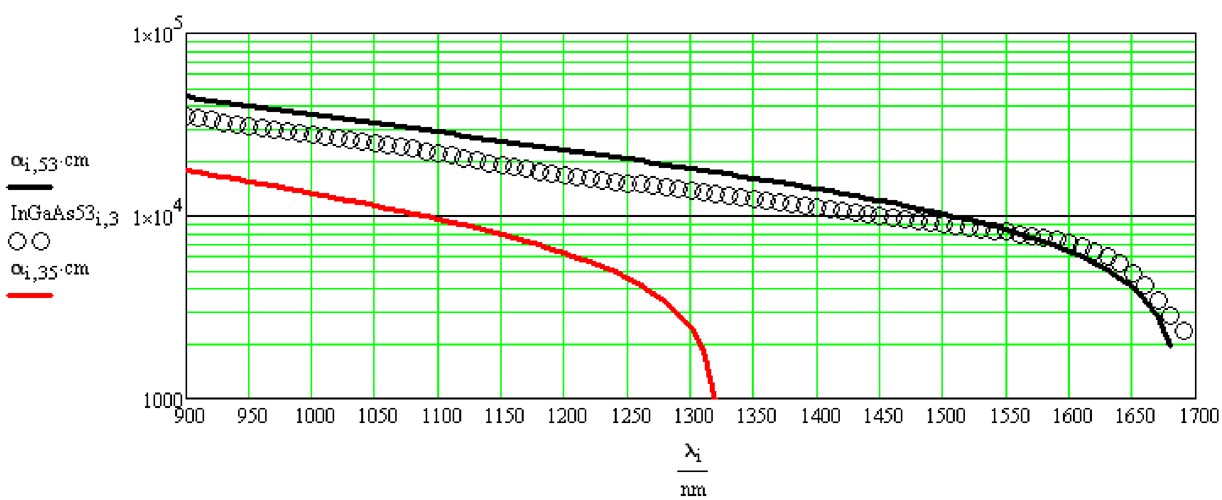

Figure 22. InGaAs absorption coefficient model used in program.

4.7.3 4.7.3 InGaAs Cell Thickness vs 1xJsc

The above absorption data was used to estimate that the bottom cell thickness to achieve the 14.2mA/cm^2 1xJsc goal of Table 1 is about 2µm (Figure 23). Although a thicker cell could generate more Jsc in theory, in practice the thickness is limited by the dislocation-limited ~1.6µm diffusion length in the uniform doped base (Figure 24) of the bottom cell as well as by wafer bow in the current cells if grown more than 2.5µm thick.

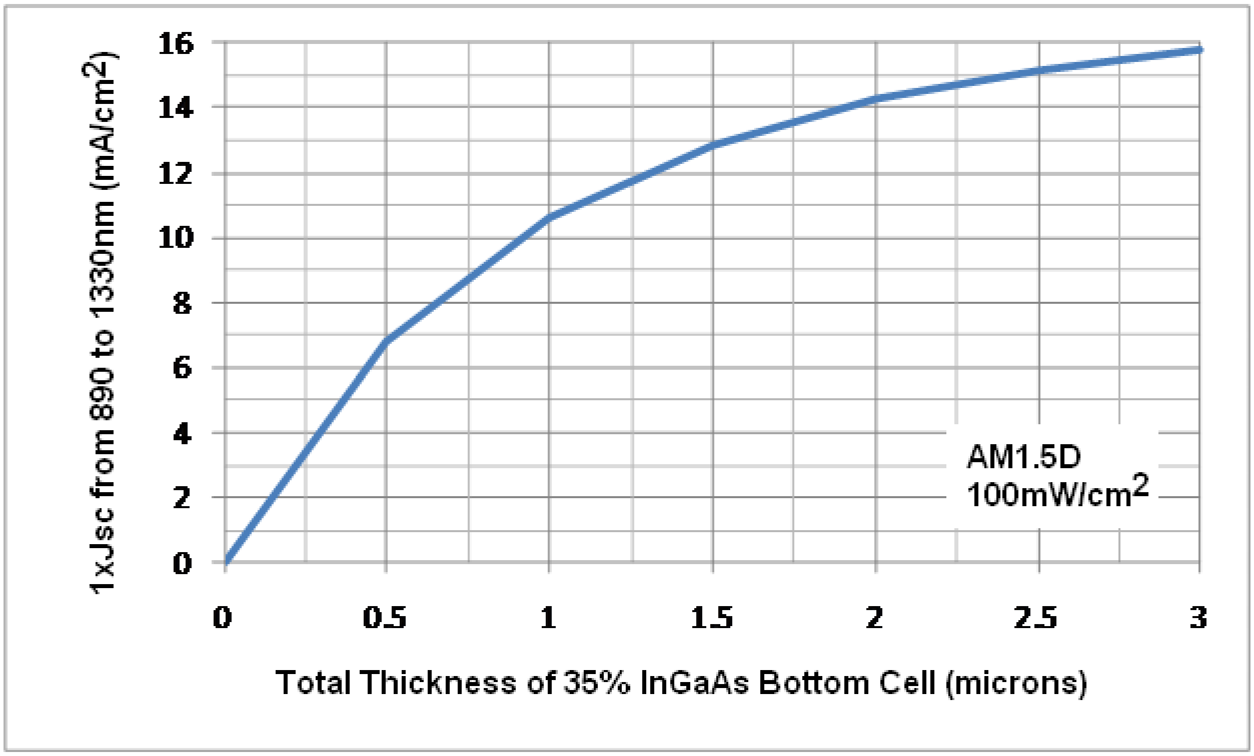

Figure 23. Calculated 1xJsc possible from InGaAs bottom cell using absorption coefficient data in Figure 22.

4.7.4 Use of a Doping Grade (Drift Field) in InGaAs Base to Enhance Diffusion Length

In order to extend the diffusion length, we graded the base doping as illustrated in Figure 24. Grading the base doping is sometimes of questionable value when the diffusion length is limited by the base doping. In the bottom cell, dislocations, not the doping, limit the lifetime and diffusion length, so a doping grade[21] can be used to good effect to generate an electric field that aids the diffusion toward the collecting junction ("downstream diffusion length").Table 6 shows the measured cell improvement with the insertion of a doping grade in the bottom cell base. The cells had the front and middle cells of a tandem grown on them and then etched off subsequently so that any degradation of the bottom cells that occurred in the tandem would occur in these test cells.

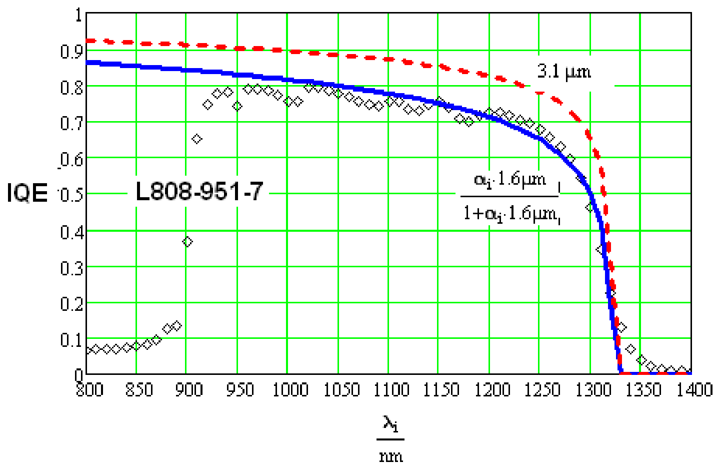

$$\mathrm{Lbase} = 1.6\ \mu\mathrm{m}$$

$$\mathrm{E} := \frac{\mathrm{k}\cdot\mathrm{Tc}}{\mathrm{q}}\cdot\frac{1}{\mathrm{Pavg}}\cdot\frac{\mathrm{p1}-\mathrm{p2}}{\mathrm{Tbase}} = 225\cdot\frac{\mathrm{V}}{\mathrm{cm}}$$

$$\mathrm{Ec} := \frac{\mathrm{k}\cdot\mathrm{Tc}}{\mathrm{q}\cdot\mathrm{Lbase}} = 161.719\cdot\frac{\mathrm{V}}{\mathrm{cm}}$$

$$\frac{1}{\frac{-1}{2\cdot\mathrm{Lbase}}\cdot\left(\frac{\mathrm{E}}{\mathrm{Ec}}\right)+\frac{1}{2\cdot\mathrm{Lbase}}\cdot\left[\left(\frac{\mathrm{E}}{\mathrm{Ec}}\right)^2+4\right]^{0.5}} = 3.1\ \mu\mathrm{m}$$

Figure 24. QE model fit (blue solid line) to measured data (open circles) for GaAs-filtered InGaAs cell with uniform base doping shows a diffusion length Lbase of ~ 1.6μm gives a good fit. Dotted curve is expected improvement from base doping grade. Short wavelength cut-on in measured data is from GaAs wafer filter (not modeled).

Table 6. Average Wafer (52 Cells) IV Data Showing InGaAs Cell Improvement with Base Doping Grade

Lot	PH_3 expose	660C anneal	Grade steps&nm/step	Base cm^{-3}	1x Jsc mA/cm^2	1x Voc V	Suns	Voc V
L829-0990-1-0992-1	yes	yes	10x250	6.0E+16	-13.6	0.372	484	0.607
L829-0991-1-0992-5	yes	yes	10x250	6e16 to 4e17	-14.1	0.394	479	0.621
In% (all): last grade step 31-window 36-emitter 35.				All emitters 300nm 5e17 cm^{-3} and bases 1700nm.				

4.7.5 *Final Bottom Cell Epistructures used in Deliveries D09, D10 and D11 and IV Data*

Table 7 shows the epistructures and single junction test data for the bottom cells used in the last three tandem deliveries (D09, D10, D11) to NREL. Insertion of a doping grade into the base did indeed help, although when a graded emitter was tried in addition to the base grading, the Jsc was not further improved (L869-1123-4-1120-7, avg 1xJsc 14.17mA/cm^2, 595mV Voc). We believe this is because the more heavily doped emitter causes some doping related recombination (possibly Auger for this lower bandgap material) as opposed to the lighter base dopings where the lifetime is mainly limited by dislocation recombination. Finally, we added a 200nm thicker final grading layer which seemed to boost the 1xJsc by 0.1mA/cm^2 and perhaps the Voc by a bit.

Table 7. Bottom Cell Epistructure Evolution and Average (52 cells) IV data

	Single Junction Test Cells all treated with upper cell growths	0953-2-0951-5 Filtered InGaAs Bottom cell **NREL: 41% 500X tandem D09**		0992-5-0991-1 Filtered InGaAs Bottom cell **NREL: 41% 500X tandem D10**		1142-8-1140-8 Filtered InGaAs Bottom cell **Spire: 43% 500X tandem D11**	
	material	Thick. nm	Doping cm^{-3}	Thick. nm	Doping cm^{-3}	Thick. nm	Doping cm^{-3}
contact cap	p $In_{0.35}Ga_{0.65}As$	600	2.0E+19	600	2.0E+19	**400**	2.0E+19
BSF	p $In_{0.36}(Al_{0.6}Ga_{0.4})_{0.64}As$	100	5.0E+17	100	5.0E+17	100	5.0E+17
base	p $In_{0.35}Ga_{0.65}As$	1700	6.0E+16	1700	**6e16 to 4e17**	1700	6e16 to 4e17
emitter	n $In_{0.35}Ga_{0.65}As$	300	5.0E+17	300	5.0E+17	300	5.0E+17
window	n $In_{0.36}(Al_{0.6}Ga_{0.4})_{0.64}As$	250	5.0E+17	250	5.0E+17	**450**	5.0E+17
grade step 9	n $In_{0.31}(Al_{0.6}Ga_{0.4})_{0.69}As$	250	4.0E+17	250	4.0E+17	250	4.0E+17
grade step 8	n $In_{0.28}(Al_{0.6}Ga_{0.4})_{0.72}As$	250	4.0E+17	250	4.0E+17	250	4.0E+17
grade step 7	n $In_{0.24}(Al_{0.6}Ga_{0.4})_{0.76}As$	250	4.0E+17	250	4.0E+17	250	4.0E+17
grade step 6	n $In_{0.21}(Al_{0.6}Ga_{0.4})_{0.79}As$	250	4.0E+17	250	4.0E+17	250	4.0E+17
grade step 5	n $In_{0.17}(Al_{0.6}Ga_{0.4})_{0.83}As$	250	4.0E+17	250	4.0E+17	250	4.0E+17
grade step 4	n $In_{0.14}(Al_{0.6}Ga_{0.4})_{0.86}As$	250	4.0E+17	250	4.0E+17	250	4.0E+17
grade step 3	n $In_{0.10}(Al_{0.6}Ga_{0.4})_{0.90}As$	250	4.0E+17	250	4.0E+17	250	4.0E+17
grade step 2	n $In_{0.07}(Al_{0.6}Ga_{0.4})_{0.93}As$	250	4.0E+17	250	4.0E+17	250	4.0E+17
grade step 1	n $In_{0.03}(Al_{0.6}Ga_{0.4})_{0.97}As$	250	4.0E+17	250	4.0E+17	250	4.0E+17
buffer	n GaAs	500	2.0E+18	150		150	2.0E+18
wafer 410	100 n GaAs 10° to 111A	650μm	1.0E+17	650μm	1.0E+17	650μm	1.0E+17
	Wafer Avg						
	1xJsc (mA/cm^2)	**13.6**		**14.11**		**14.24**	
	500xVoc (V)	**0.573**		**0.621**		**0.622**	

4.8 Tandem Cell Data

In the above sections, we have extensively discussed single junction InGaP top, GaAs middle, and InGaAs bottom cells, and tunnel junctions where a great deal of care went into optically filtering and heat treating them as they would be in the final tandem. We believe much of the quick progress we made in this program occurred due to this experimental approach in which it was easy to decipher problems in single junction cells than in multijunction cells. The Table 1 roadmap indicates the tandem cell performance is well predicted by this method. Therefore, in this section, we will primarily discuss the tandem results with less analysis (see the sections on the individual subcells for that).

4.8.1 Tandem Illuminated IV Data

Figure 25 shows the illuminated IV data as measured by NREL for tandems in D09 and D10. For the 5,5mm cells from D10 (Fig. 25a), the average lot efficiency of 1780 cells was 39.9% at 500X as measured by Spire Semiconductor, with the best cell measured as 42%. NREL measured the best cell as 41.4%. Measurements agree within NREL's stated error. Figure 19b shows a larger 1cm^2 cell NREL has measured from D09 as 41.0% at 500X, although the efficiency was slightly higher at the lower concentration shown. The one sun Jsc's (1xJsc) shown were calculated from the NREL supplied data. Figure 1 in the Executive Summary is the NREL illuminated IV for the record cell from D11.

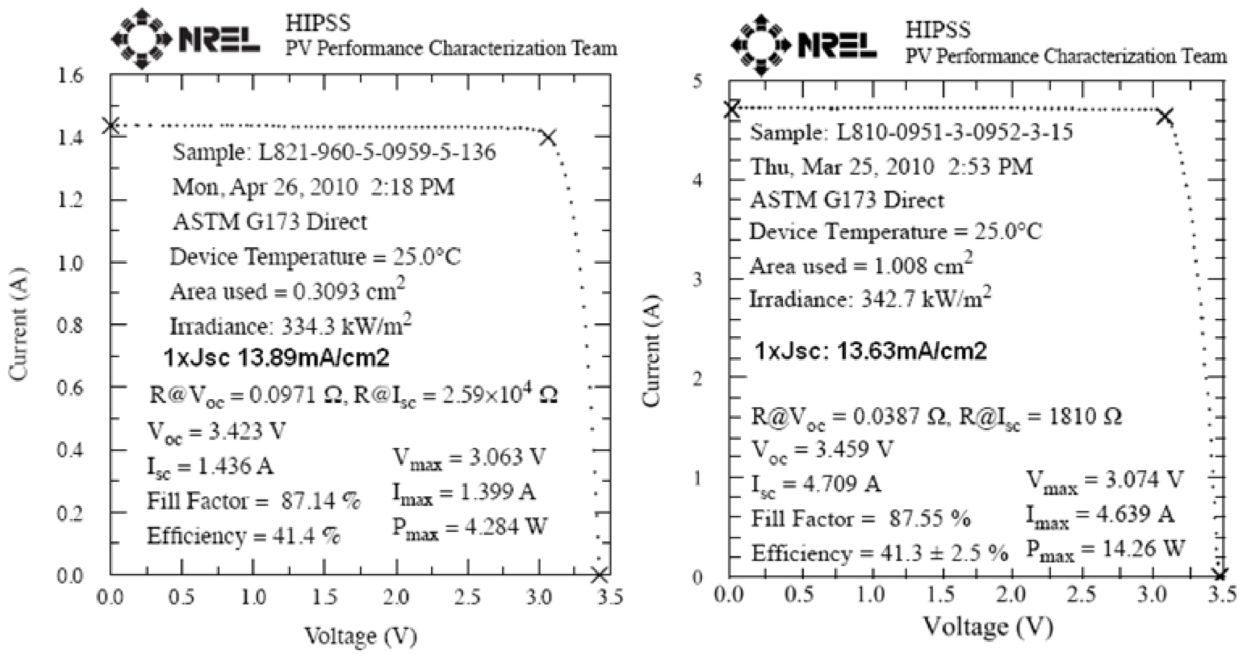

Figure 25. a) Left: 5.5mm 3-junction cell. Epistructure as in Table 3. B) Right: 1cm 3-junction cell.

Essentially no large improvement was made from D9 to D10; where the only significant epi change was the use of a doping grade in the bottom cell to increase its Jsc. This alone was not enough to move the efficiency significantly (despite what tandem QE data shows, the InGaAs bottom cell was not limiting the Jsc).

We attribute the 1% point efficiency bump in the D11 cells to the significant epistructure changes to all three subcells (shown in Table 2) which were all geared towards increasing the 1xJsc of each subcell: InGaP top cell – thicker base and strained window; GaAs middle cell – thicker base and 1%InGaAs absorber region; InGaAs bottom cell – graded base doping to increase diffusion lengths and slightly thicker final step (window) in grading layer (dislocation reduction) stack.

4.8.2 Tandem QE Data

Figure 26 shows a measured tandem external QE from NREL for a typical bi-facial cell. We have appended a Spire-measured reflectance curve that was taken for this wafer after the MgF_2/ZnS coating deposition, as well as the NREL IV data for this tandem (at 281X). The 1xJsc obtained for each subcell was obtained by integrating the NREL QE data with the AM1.5D spectrum with the power normalized to 100mW/cm^2. This particular tandem appears to be top-cell current limited. The small gap between the GaAs middle cell and InGaAs bottom cells is of most interest and is due to the GaAs wafer absorption discussed earlier. We compensate for this loss by extending the InGaAs cutoff wavelength as needed. Figure 27 shows Spire-measured external QE for the single-junction subcells employed for the final tandem with a 120nmMgF_2/60nm ZnS coating deposition, The 1xJsc obtained for each subcell was well matched.

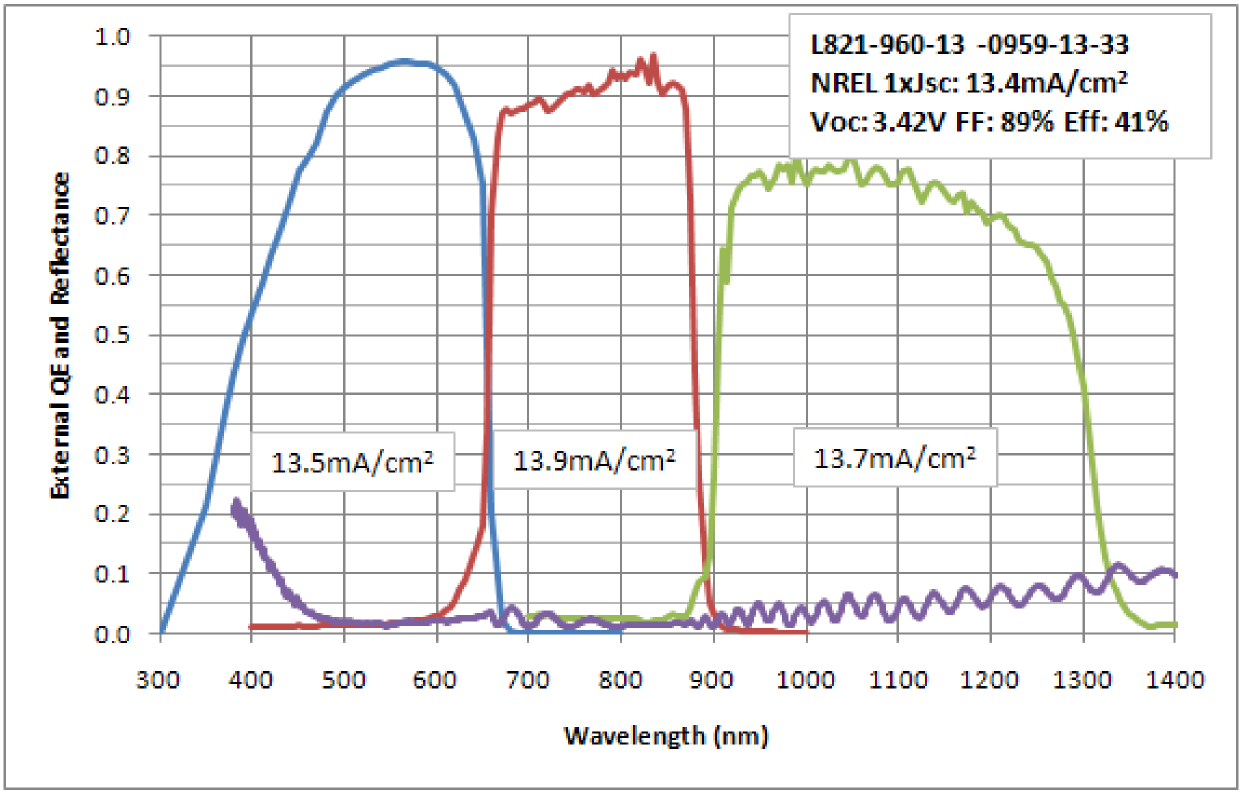

Figure 26. NREL-measured external tandem QE showing response of InGaP, GaAs, and InGaAs subcells and Spire-measured reflectance of a bi-facial tandem.

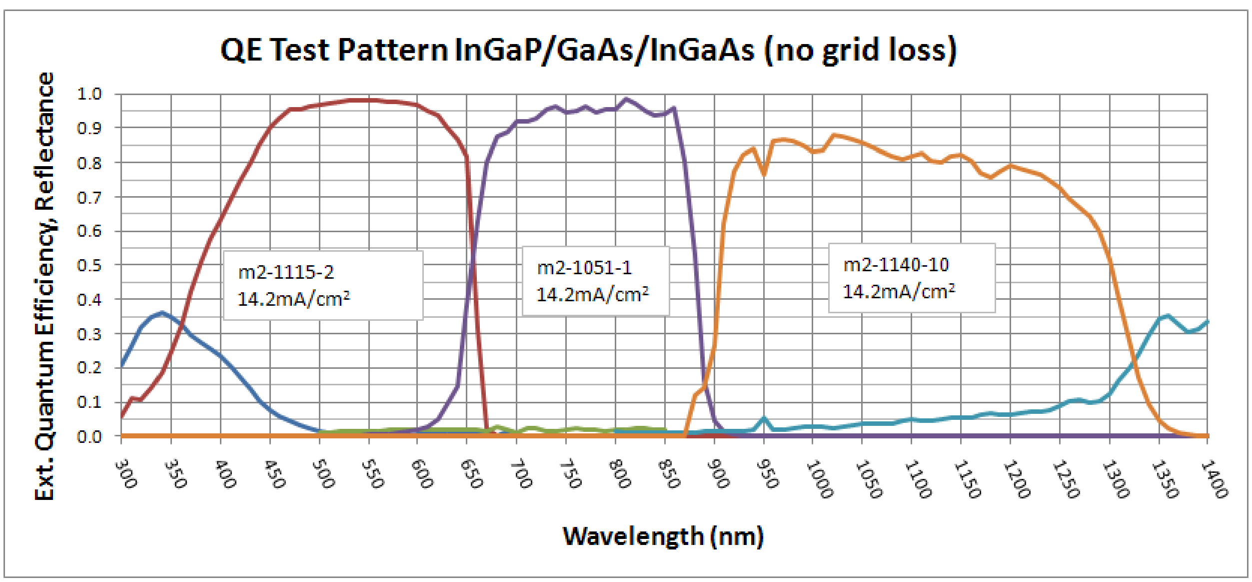

Figure 27. Spire-measured external QE of single junction InGaP, GaAs, and InGaAs test subcells used in final D11 delivery.

4.8.3 Final D11 Epistructure

The final program epistructure is shown in Table 2 above. The InGaP top cells is thicker (1.4µm base) and has a doping-graded emitter (perhaps a 1xJsc gain of +0.15mA/cm^2, L847 1047-2 vs 1043-2) and strained higher bandgap InAlP window (perhaps +0.1mA/cm^2, L847 1065-1 vs 1043-2), the GaAs middle cell has the 1% InGaAs absorber added at the back of the cell, and the bottom cell utilizes a doping grade in the base and a slightly thicker final step of the grade.

5 Commercialization Efforts

5.1 Burn-In Data at 85C 200Hrs

Table 8 shows 85C 200 hour burn-in data on ten randomly selected 3 junction tandems. The test was within the 10% spec set by NREL. Most of the degradation is from one bad cell (cell 13, of course) that went from 39 to 34%. Structurally, the cells have not changed much in the more recent deliveries, so we believe the reliability data is still useful. The final D11 cells with the "pseudomorphic" 1%InGaAs were checked at 85C for 48hrs and showed no degradation (Table 9). A shorter burn-in time was used simply because we were near the end of the program, and was done simply because we wanted to at least know that the final cells seemed stable. We have detailed specifications from Amonix for tests the cells have to meet in order for them to be put on-sun by Amonix. The end of the program was dedicated to reaching the efficiency target. We will now have some time to set up the reliability tests needed by module makers as we pursue commercial opportunities with these bi-facial growth cells.

Table 8. Tandem 85C 200hr Burn-In Data on Early Tandems

L748-		Before 85C 200hr Burn-in					After 85C 200hr Burn-in					Performance	
860-6-	cell	1xJsc	Jsc	Voc	FF	Eff	1xJsc	Jsc	Voc	FF	Eff	change	
858-3		mA/cm^2	A/cm^2	V			mA/cm^2	A/cm^2	V				
	1	13.36	6.637	3.384	0.855	0.387	13.41	6.414	3.374	0.846	0.383	ΔEff/Eff	-3.9%
	4	13.13	6.605	3.371	0.867	0.384	13.05	6.411	3.365	0.849	0.373	ΔVoc/Voc	-0.3%
	5	12.85	6.417	3.390	0.880	0.384	13.05	6.476	3.380	0.850	0.375	Δ1xJsc/1xJsc	-1.5%
	8	12.80	6.497	3.384	0.882	0.382	12.78	6.517	3.381	0.833	0.360	ΔFF/FF	-2.1%
	9	12.94	6.403	3.356	0.859	0.373	12.87	6.319	3.345	0.846	0.364		
	13	12.98	6.505	3.364	0.885	0.386	12.08	6.291	3.345	0.848	0.343		
	14	12.97	6.406	3.353	0.855	0.372	12.09	6.164	3.338	0.857	0.346		
	16	13.02	6.536	3.369	0.876	0.384	12.91	6.369	3.357	0.868	0.376		
	18	12.95	6.404	3.354	0.858	0.373	12.83	6.275	3.340	0.845	0.362		
	20	13.09	6.544	3.358	0.849	0.373	13.00	6.365	3.351	0.843	0.367		
average		13.01	6.495	3.368	0.867	0.380	12.81	6.360	3.358	0.848	0.365		
std dev		0.16	0.086	0.014	0.013	0.006	0.42	0.103	0.016	0.009	0.013		

Table 9. Tandem 85C 48hr Burn-In Data on Final (D11) Tandems

	5.5mm cells	Jsc A/cm2	Voc V	Vm V	Pm W	FF	conc. Suns	Efficiency
	average	6.809	3.455	3.058	20.244	0.860	471.0	0.430
0 hrs	stdev	0.083	0.009	0.024	0.347	0.008	4.5	0.005
	median	6.782	3.455	3.061	20.199	0.862	471.5	0.430
	count	35	35	35	35	35	35	35
48hrs	average	6.811	3.458	3.067	20.337	0.864	471.5	0.431
85C	stdev	0.090	0.008	0.030	0.378	0.009	4.1	0.005
	median	6.797	3.458	3.069	20.300	0.863	471.6	0.430
	count	35	35	35	35	35	35	35

5.2 Commercial Companies Evaluating Spire Tandems

Companies evaluating Spire cells in modules are:

- Morgan Solar
- BrightLeaf (was Aquasoladyne)

Companies evaluating Spire cells for possible use in modules are:

- Soliant
- SolFocus
- Amonix

All of the above companies have Spire Semiconductor cell samples, but the latter group requires more reliability data than we currently have at this point to start module tests.

6 Spire SAI Program Team

Management: Ed Gagnon, Vic Haven
Business Development: Brad Siskavich
Epigrowth: Phillip Chiu, Xuebing Zhang, Steve Markham, Tri Ta
Wafer Process: Chris Harris, Daryl Pulver, Dan Stevens, Nathan Bonniah, Yungeng Gao
Cell Test: Phillip Chiu, Daniel Derkacs
Device Design and Modeling: Steve Wojtczuk, Daniel Derkacs
Independent Consultant: Mike Timmons
Principal Investigator: Steve Wojtczuk

7 References

[1] S. Wojtczuk, P. Chiu, X. Zhang, D. Derkacs, C. Harris, D. Pulver, and M. Timmons, "InGaP/GaAs/InGaAs 41% Concentrator Cells Using Bi-Facial Epigrowth," Proc. of the 35th IEEE Photovoltaic Specialists Conf., Honolulu, HI 2010 (to be published).

[2] J.M. Olson, S.R. Kurtz, A.E. Kibbler, and P. Faine, "A 27.3%. Efficient Ga(0.5)In(0.5)P/GaAs Tandem Solar Cell," Appl. Phys. Lett., 56, 1990, pp. 623-625.

[3] R.R. King, A. Boca, W. Hong, X.Q. Liu, D. Bhusari, D. Larrabee, K.M. Edmondson, D.C. Law, C.M.Fetzer, S. Mesropian, and N.H. Karam, "Band-Gap Engineering Architectures for High-Efficiency Multijunction Concentrator Solar Cells," 24th European Photovoltaic Solar Energy Conference, 2009, pp. 55-61.

[4] W. Guter, J. Schöne, S.P. Philipps, M. Steiner, G. Siefer, A. Wekkeli, E. Welser, E. Oliva, A.W. Bett, and F. Dimroth, "Current-matched triple-junction solar cell reaching 41.1% conversion efficiency under concentrated sunlight" , *Appl. Phys. Lett*., **94**, 223504 (2009)

[5] J. F. Geisz, D. J. Friedman, J. S. Ward, A. Duda, W. J. Olavarria, T. E. Moriarty, J. T. Kiehl, M. J. Romero, A. G. Norman, and K. M. Jones, "40.8% efficient inverted triple-junction solar cell with two independently metamorphic junctions," *Appl. Phys. Lett.* **93**, 123505 (2008).

[6] Barnett, A.; Honsberg, C.; Kirkpatrick, D.; Kurtz, S.; Moore, D.; Salzman, D.; Schwartz, R.; Gray, J.; Bowden, S.; Goossen, K.; Haney, M.; Aiken, D.; Wanlass, M.; Emery, K, "50% Efficient Solar Cell Architectures and Designs", Conference Record of the 2006 IEEE 4th World Conference on Photovoltaic Energy Conversion, Volume 2, May 2006 pp. 2560-2564.

[7] J.C. Schultz, M.E. Klausmeier-Brown, M. Ladle-Ristow and M.M. Al-Jassim "High Efficiency 1.0eV GaInAs Bottom Solar Cell for 3-Junction Monolithic Stack", Conf. Rec. of 21st IEEE PVSC, 1990, pp.148-152.

[8] R. King et al. "Pathways to 40% Efficient Concentrator Photovoltaics" 20th European Solar Energy Conf. 2005, pp. 118–123.

[9] M. Wanlass, "Low Bandgap, Monolithic, Multi-Bandgap, Optoelectronic Devices," Pat. App. US2006/0162768 A1.

[10] C.H. Henry, "Limiting efficiencies of ideal single and multiple energy gap terrestrial solar cells," J. Appl. Phys. **51**(8), 1980, pp. 4494-4500.

[11] M.A. Green, ***Solar Cells***, Prentice-Hall, 1982, pp. 96-97.

[12] W.G. Spitzer and J. M. Whelan, Phys. Rev. 114, 1 (1959) pp. 59-63.

[13] ***Handbook of Optical Constants of Solids,*** E.D. Palik, Ed., Academic Press, 1985, pp.429-433.

[14] S.R. Kurtz, J.M. Olson, D.J. Arent, A.E. Kibbler, and K.A. Bertness, "Competing Kinetic and Thermodynamic Processes in the Growth and Ordering of $Ga_{0.5}In_{0.5}P$," Mat. Res. Soc. Symp. Proc. Vol. 312.

[15] R. Ferrini et al., "Optical functions of InGaP/GaAs epitaxial layers from 0.01 to 5.5eV," Eur. Phys. J. B 27, 2002, pp. 449-458.

[16] D. H. Levi, J. Geisz, and B. Johs "Effects of ordering on the optical properties of GaInP2" Proc. SPIE, Vol. 5530, 326 (2004);

[17] Private communication.

[18] J.W. Matthews and A.E. Blakeslee, J. Cryst. Growth 27, 1974, pp.118.

[19] S. Wang, ***Fundamentals of Semiconductor Theory and Device Physics***, Prentice-Hall, 1989, pp. 486-492.

[20] E. Rosencher and B. Vintner, ***Optoelectronics***, Cambridge University Press, 2002, pp. 312-313.

[21] A.L. Fahrenbruch and R.H. Bube, ***Fundamentals of Solar Cells***, Academic Press, 1983, pp. 83-84.